



PUBLISHED FOR SISSA BY SPRINGER

RECEIVED: January 8, 2016

REVISED: January 26, 2016

ACCEPTED: February 4, 2016

PUBLISHED: February 19, 2016

Study of $D_{sJ}^{(*)+}$ mesons decaying to $D^{*+}K_S^0$ and $D^{*0}K^+$ final states



The LHCb collaboration

E-mail: antimo.palano@ba.infn.it

ABSTRACT: A search is performed for $D_{sJ}^{(*)+}$ mesons in the reactions $pp \rightarrow D^{*+}K_S^0 X$ and $pp \rightarrow D^{*0}K^+ X$ using data collected at centre-of-mass energies of 7 and 8 TeV with the LHCb detector. For the $D^{*+}K_S^0$ final state, the decays $D^{*+} \rightarrow D^0\pi^+$ with $D^0 \rightarrow K^-\pi^+$ and $D^0 \rightarrow K^-\pi^+\pi^+\pi^-$ are used. For $D^{*0}K^+$, the decay $D^{*0} \rightarrow D^0\pi^0$ with $D^0 \rightarrow K^-\pi^+$ is used. A prominent $D_{s1}(2536)^+$ signal is observed in both $D^{*+}K_S^0$ and $D^{*0}K^+$ final states. The resonances $D_{s1}^*(2700)^+$ and $D_{s3}^*(2860)^+$ are also observed, yielding information on their properties, including spin-parity assignments. The decay $D_{s2}^*(2573)^+ \rightarrow D^{*+}K_S^0$ is observed for the first time, at a significance of 6.9σ , and its branching fraction relative to the $D_{s2}^*(2573)^+ \rightarrow D^+K_S^0$ decay mode is measured.

KEYWORDS: Hadron-Hadron scattering, Charm physics

ARXIV EPRINT: [1601.01495](https://arxiv.org/abs/1601.01495)

Contents

1	Introduction	1
2	Detector and simulation	2
3	Event selection	3
4	Mass spectra	6
5	Measurement of the branching fraction of the decay $D_{s2}^{*+}(2573)^+ \rightarrow D^{*+}K_s^0$	11
6	Spin-parity analysis of the $D^{*+}K_s^0$ system	16
7	Summary	17
	The LHCb collaboration	21

1 Introduction

The discovery by the BaBar collaboration of a narrow state $D_{s0}^{*+}(2317)^+$ in the decay to $D_s^+\pi^0$ [1], and the subsequent discovery of a second narrow particle, $D_{s1}(2460)^+$ in the decay to $D_s^{*+}\pi^0$ [2–4], raised considerable interest in the spectroscopy of heavy mesons.¹ These discoveries were a surprise because quark model calculations based on heavy quark effective theory (HQET) [5] predicted the masses of these resonances to be above the DK and D^*K thresholds, respectively.² Consequently their widths were expected to be very large, as for the corresponding $J^P = 0^+$ and $J^P = 1^+$ resonances in the D_J spectrum.

The D_{sJ}^{*+} mesons are expected to decay into the DK and D^*K final states if they are above threshold. The BaBar collaboration has explored the DK and D^*K mass spectra [6, 7] observing two states, $D_{sJ}^{*+}(2700)^+$ and $D_{sJ}^{*+}(2860)^+$, both decaying to DK and D^*K with a natural parity (NP) assignment.³ A third structure, $D_{sJ}(3040)^+$, is observed only in the D^*K decay mode with a preferred unnatural parity (UP) assignment. The $D_{sJ}^{*+}(2700)^+$ resonance was also observed by the Belle and BaBar collaborations in a study of B decays to $D\bar{D}K$ [8, 9]. Both collaborations obtain a spin-parity assignment $J^P = 1^-$ for this state, and so it is labelled as $D_{s1}^{*+}(2700)^+$.

The LHCb experiment has performed studies of the DK final states in the inclusive process, $pp \rightarrow DKX$ [10], and in the Dalitz plot analysis of $B_s^0 \rightarrow \bar{D}^0 K^- \pi^+$ decays [11, 12].

¹The inclusion of charge-conjugate processes is implied, unless stated otherwise.

²In the following D^* is a generic label to indicate the ground state $D^*(2010)^+$ or $D^*(2007)^0$ resonances.

³States having $P = (-1)^J$ and therefore $J^P = 0^+, 1^-, 2^+, \dots$ are referred as natural parity states and are labelled as D^* , while unnatural parity indicates the series $J^P = 0^-, 1^+, 2^-, \dots$

In the inclusive analysis, the $D_{s1}^*(2700)^+$ and $D_{sJ}^*(2860)^+$ are observed with large statistical significance and their properties are found to be in agreement with previous measurements. In the exclusive Dalitz plot analysis of the $B_s^0 \rightarrow \bar{D}^0 K^- \pi^+$ decays, the $\bar{D}^0 K^-$ mass spectrum shows a complex resonant structure in the 2860 MeV mass region.⁴ This is described by a superposition of a broad $J^P = 1^-$ resonance and a narrow $J^P = 3^-$ resonance with no evidence for the production of $D_{s1}^*(2700)^-$. Since the narrow structure at 2860 MeV seen in inclusive DK and D^*K analyses could contain contributions from various resonances with different spins, it is labelled as $D_{sJ}^*(2860)^+$.

In references [13–18] attempts are made to identify these states within the quark model and in ref. [19] within molecular models. The expected spectrum for D_s^+ mesons has recently been recomputed in refs. [20, 21]. In particular, ref. [20] points out that six states are expected in the mass region between 2.7 and 3.0 GeV. To date, evidence has been found for three of the states; hence finding the rest would provide an important test of these models. In this paper we study the $D^{*+}K_S^0$ and $D^{*0}K^+$ systems using pp collision data, collected at centre-of-mass energies of 7 and 8 TeV with the LHCb detector.

2 Detector and simulation

The LHCb detector [22, 23] is a single-arm forward spectrometer covering the pseudorapidity range $2 < \eta < 5$, designed for the study of particles containing b or c quarks. The detector includes a high-precision tracking system consisting of a silicon-strip vertex detector surrounding the pp interaction region, a large-area silicon-strip detector located upstream of a dipole magnet with a bending power of about 4 Tm, and three stations of silicon-strip detectors and straw drift tubes placed downstream of the magnet. The tracking system provides a measurement of momentum, p , of charged particles with a relative uncertainty that varies from 0.5% at low momentum to 1.0% at 200 GeV. The minimum distance of a track to a primary vertex (PV), the impact parameter, is measured with a resolution of $(15 + 29/p_T) \mu\text{m}$, where p_T is the component of the momentum transverse to the beam, in GeV. Different types of charged hadrons are distinguished using information from two ring-imaging Cherenkov detectors (RICH). Photons, electrons and hadrons are identified by a calorimeter system consisting of scintillating-pad and preshower detectors, an electromagnetic calorimeter and a hadronic calorimeter. Muons are identified by a system composed of alternating layers of iron and multiwire proportional chambers. The online event selection is performed by a trigger, which consists of a hardware stage, based on information from the calorimeter and muon systems, followed by a software stage, which applies a full event reconstruction.

In the simulation, pp collisions are generated using PYTHIA [24] with a specific LHCb configuration [25]. Decays of hadronic particles are described by EVTGEN [26], in which final-state radiation is generated using PHOTOS [27]. The interaction of the generated particles with the detector, and its response, are implemented using the GEANT4 toolkit [28] as described in ref. [29]. We also make use of simple generator-level simulations [30] to study kinematic effects.

⁴Natural units are used throughout the paper.

3 Event selection

We search for $D_{sJ}^{(*)+}$ mesons using the inclusive reactions

$$pp \rightarrow D^{*+} K_s^0 X \quad (3.1)$$

and

$$pp \rightarrow D^{*0} K^+ X, \quad (3.2)$$

where X represents a system composed of any collection of charged and neutral particles. Use is made of both 7 and 8 TeV data for reaction (3.1), corresponding to an integrated luminosity of 3 fb^{-1} , and 8 TeV data only for reaction (3.2) which corresponds to an integrated luminosity of 2 fb^{-1} .

The charmed mesons in the final state are reconstructed in the decay modes $D^{*+} \rightarrow D^0 \pi^+$, with $D^0 \rightarrow K^- \pi^+$ and $D^0 \rightarrow K^- \pi^+ \pi^+ \pi^-$, and $D^{*0} \rightarrow D^0 \pi^0$, with $D^0 \rightarrow K^- \pi^+$ and $\pi^0 \rightarrow \gamma\gamma$. The K_s^0 mesons are reconstructed in their $K_s^0 \rightarrow \pi^+ \pi^-$ decay mode. Because of their long lifetime, K_s^0 mesons may decay inside or outside the vertex detector. Candidate K_s^0 mesons that are reconstructed using vertex detector information are referred to as “long” while those reconstructed without vertex detector information are called “down-stream”. Those that decay within the vertex detector acceptance have a mass resolution about half as large as those that decay outside of its acceptance. Reaction (3.1) with $D^0 \rightarrow K^- \pi^+$ serves as the primary channel for studying the $D_{sJ}^{(*)+}$ resonance structures and their parameters, while reaction (3.1) with $D^0 \rightarrow K^- \pi^+ \pi^+ \pi^-$ and reaction (3.2) are used for cross-checks and to confirm the observed signatures.

Charged tracks are required to have good track fit quality, momentum $p > 3 \text{ GeV}$ and $p_T > 250 \text{ MeV}$. These conditions are relaxed to $p > 1 \text{ GeV}$ and $p_T > 150 \text{ MeV}$ for the “soft” pion originating directly from the D^{*+} decay. In the reconstruction of the D^0 candidates we remove candidate tracks pointing to a PV, using an impact parameter requirement. All tracks used to reconstruct the D mesons are required to be consistent with forming a common vertex and the D meson candidate must be consistent with being produced at a PV. The D^{*+} and K_s^0 , and similarly the D^0 and K^+ candidates, are fitted to a common vertex, for which a good quality fit is required. The purity of the charmed meson sample is enhanced by requiring the decay products to be identified by the particle identification system, using the difference in the log-likelihood between the kaon and pion hypotheses $\Delta \ln \mathcal{L}_{K\pi}$ [31]. We impose a tight requirement of $\Delta \ln \mathcal{L}_{K\pi} > 3$ for kaon tracks and a loose requirement of $\Delta \ln \mathcal{L}_{K\pi} < 10$ for pions. The overlap region in the particle identification definition of a kaon and a pion is small and does not affect the measured yields, given the small number of multiple candidates per event.

Candidate D^0 mesons are required to be within $\pm 2.5\sigma$ of the fitted D^0 mass where the mass resolution σ is 8.3 MeV. The $D^0 \pi^+$ invariant mass is computed as

$$m(D^0 \pi^+) = m(K^- \pi^+ \pi^+) - m(K^- \pi^+) + m_{D^0}, \quad (3.3)$$

where m_{D^0} is the world average value of the D^0 mass [32]. For the channel $D^0 \rightarrow K^- \pi^+ \pi^+ \pi^-$, the invariant mass $m(D^0 \pi^+)$ is defined similarly.

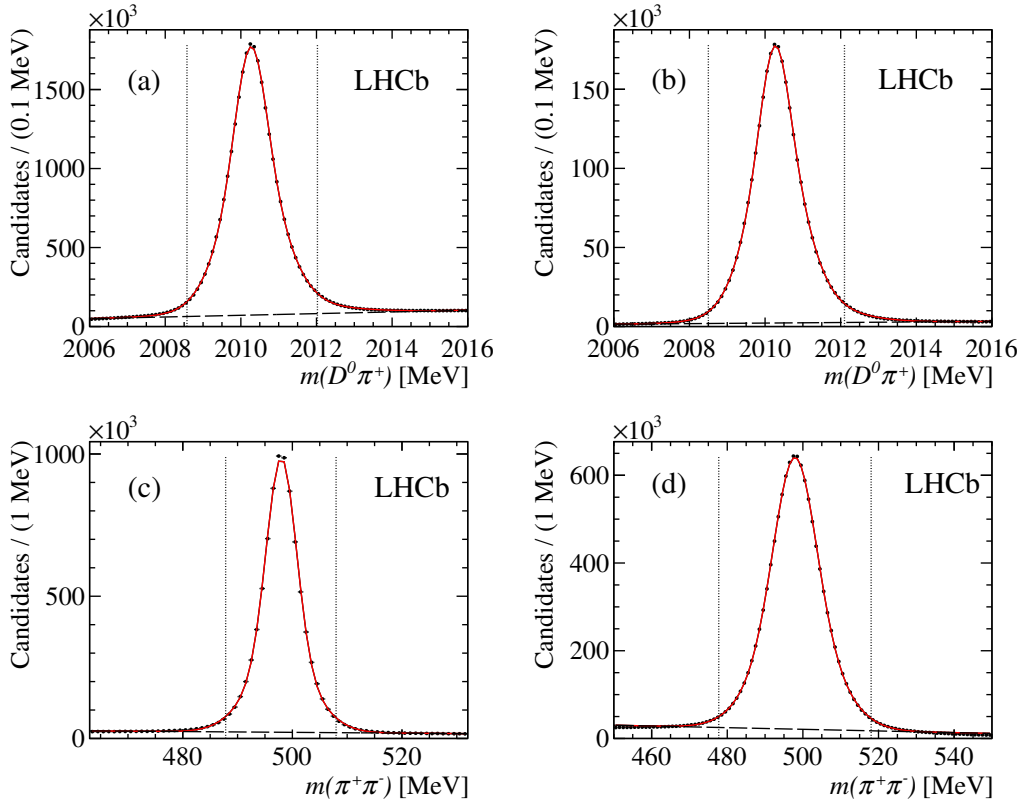


Figure 1. Distributions of $D^0\pi^+$ invariant mass for (a) $D^0 \rightarrow K^-\pi^+$ and (b) $D^0 \rightarrow K^-\pi^+\pi^+\pi^-$. $\pi^+\pi^-$ mass spectrum for (c) long and (d) downstream K_S^0 . The full (red) lines describe the fitting function. The dashed lines show the background contributions and the vertical dotted lines indicate the signal regions.

Figure 1 shows the $D^0\pi^+$ invariant mass spectrum for (a) $D^0 \rightarrow K^-\pi^+$ and (b) $D^0 \rightarrow K^-\pi^+\pi^+\pi^-$. Clean D^{*+} signals for both D^0 decay modes are observed. We fit the mass spectra using the sum of a Gaussian function for the signal and a second-order polynomial for the background. The signal regions are defined to be within $\pm 2.5\sigma$ of the peak values, where $\sigma = 0.7$ MeV for both channels.

The $\pi^+\pi^-$ mass spectra for the two K_S^0 types, the long K_S^0 and downstream K_S^0 , are shown in figures 1(c) and 1(d) and are fitted using the same model as for the $D^0\pi^+$ invariant masses. The signal regions are similarly defined within $\pm 2.5\sigma$ of the peak, with $\sigma = 4.1$ MeV and 8.7 MeV for long and downstream K_S^0 , respectively.

The π^0 candidates are obtained by kinematically fitting to a π^0 hypothesis each pair of photon candidates with energy greater than 600 MeV, with the diphoton mass constrained to the nominal π^0 mass [32]. Candidate D^{*0} mesons are formed by combining $D^0 \rightarrow K^-\pi^+$ decays with all π^0 candidates in the event that have $p_T > 450$ MeV. The resulting D^{*0} candidate is required to have $p_T > 6000$ MeV. Figure 2 shows the $\Delta m(D^0\pi^0) = m(K^-\pi^+\pi^0) - m(K^-\pi^+)$ distribution, where a clear D^{*0} signal can be seen. The mass spectrum is fitted using for background the threshold function

$$B(m) = P(m)(m - m_{th})^\alpha e^{-\beta m - \gamma m^2}, \quad (3.4)$$

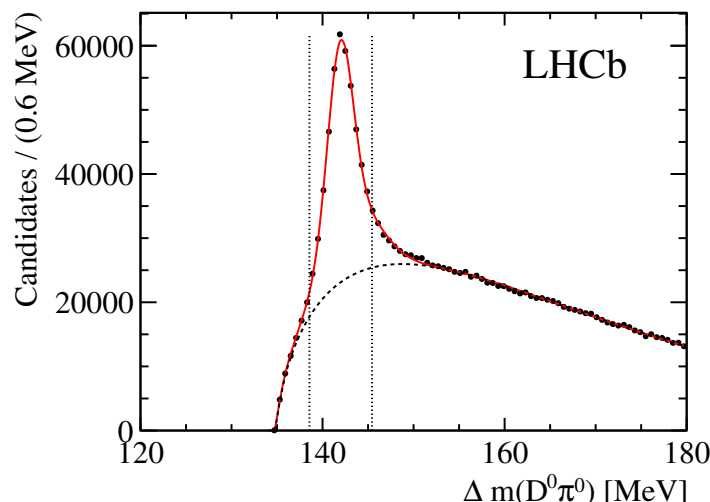


Figure 2. Distribution of $\Delta m(D^0\pi^0)$ invariant mass. The full (red) line describes the fitting function. The dashed line show the background contribution and the dotted vertical lines define the D^{*0} signal region.

where in this case $m = \Delta m(D^0\pi^0)$, m_{th} is the $\Delta m(D^0\pi^0)$ threshold mass and α , β and γ are free parameters. In eq. (3.4) $P(m)$ is the center of mass momentum of the two-body decay of a particle of mass m into two particles with masses m_1 and m_2 ,

$$P(m) = \frac{1}{2m} \sqrt{[m^2 - (m_1 + m_2)^2][m^2 - (m_1 - m_2)^2]}. \quad (3.5)$$

The function $B(m)$ gives the correct behaviour of the fit at threshold. The D^{*0} signal is modelled using the sum of two Gaussian functions. We select the candidates in the $\pm 2\sigma$ window around the peak, where $\sigma = 1.72$ MeV is the width of the dominant Gaussian fitting function, and we form D^*K pairings by combining D^{*+} and K_S^0 candidates for reaction (3.1), and D^{*0} and K^+ candidates for reaction (3.2).

To suppress the large combinatorial background, a set of additional criteria is applied. We define θ as the angle between the momentum direction of the kaon in the D^*K rest frame and the momentum direction of the D^*K system in the laboratory frame. Whereas the signal events are expected to be symmetrically distributed in the variable $\cos\theta$, after correcting for efficiency, more than 90% of the combinatorial background is found in the negative $\cos\theta$ region. The $\cos\theta$ requirements are optimized using the $D_{s1}^*(2700)^+$ signal, an established resonance. We fit the D^*K mass spectra (using the model described below) with different $\cos\theta$ selections and obtain the yields for $D_{s1}^*(2700)^+$ signal (N_S) and background events (N_B) in the $D_{s1}^*(2700)^+$ signal region (defined in the window $|m(D^*K) - m(D_{s1}^*(2700)^+)| < \Gamma(D_{s1}^*(2700)^+)/2$). We compute the signal significance $S = N_S/\sqrt{N_S + N_B}$ and signal purity $P = N_S/(N_S + N_B)$ and find that the requirements $\cos\theta > 0$ (for $D^{*+}K_S^0$, $D^0 \rightarrow K^-\pi^+$), $\cos\theta > -0.15$ (for $D^{*+}K_S^0$, $D^0 \rightarrow K^-\pi^+\pi^+\pi^-$) and $\cos\theta > -0.1$ (for $D^{*0}K^+$) each provide a good compromise between significance and purity in the respective channel. With the same method it is also found that it is optimal to

require $p_T > 4000$ MeV for all three final states. Simulations show that the mass resolution is much smaller than the natural widths of the resonances.

The analysis of the D^*K system, with $D^* \rightarrow D\pi$, is a three-body decay and therefore allows a spin analysis of the produced resonances and a separation of the different spin-parity components. We define the helicity angle θ_H as the angle between the K_S^0 and the π^+ from the D^{*+} decay, in the rest frame of the $D^{*+}K_S^0$ system. Simulated events are used to determine the efficiency as a function of $\cos\theta_H$, which is found to be uniform only for the $D^{*+}K_S^0$ candidates formed from the downstream K_S^0 sample. Therefore, for studying the angular distributions we do not use the long K_S^0 sample, which removes approximately 30% of the data.

4 Mass spectra

In order to improve the mass resolution on the D^*K mass spectra, we compute the D^{*+} , K_S^0 and D^{*0} energies using the world average mass measurements [32]. The $D^{*+}K_S^0$ mass spectrum for $D^0 \rightarrow K^-\pi^+$ is shown in figure 3 and contains 5.72×10^5 combinations. We observe a strong $D_{s1}(2536)^+$ signal and weaker resonant contributions due to $D_{s2}^*(2573)^+$, $D_{s1}^*(2700)^+$, and $D_{sJ}^*(2860)^+$ states. The $D_{s2}^*(2573)^+$ decay to $D^{*+}K_S^0$ is observed for the first time. A binned χ^2 fit to the mass spectrum is performed in which the narrow $D_{s1}(2536)^+$ is described by a Gaussian function with free parameters. Other resonances are described by relativistic Breit-Wigner (BW) functions (in D -, P - and F -wave for $D_{s2}^*(2573)^+$, $D_{s1}^*(2700)^+$, and $D_{s3}^*(2860)^+$ respectively).

Using the definition of the center-of-mass momentum $P(m)$ given in eq. (3.5), we parameterize the BW function for a resonance of mass M as

$$BW(m) = \frac{P(m) \left(\frac{P(m)}{P(M)} \right)^{2L} \frac{D^2(P(M))}{D^2(P(m))}}{(m^2 - M^2)^2 + M^2 \Gamma^2(m)}, \quad (4.1)$$

where

$$\Gamma(m) = \Gamma \frac{M}{m} \left(\frac{P(m)}{P(M)} \right)^{2L+1} \frac{D^2(P(M))}{D^2(P(m))}, \quad (4.2)$$

and

$$D(P) = \begin{cases} \sqrt{1 + (PR)^2} & \text{for } L = 1, \\ \sqrt{9 + 3(PR)^2 + (PR)^4} & \text{for } L = 2, \\ \sqrt{225 + 45(PR)^2 + 6(PR)^4 + (PR)^6} & \text{for } L = 3, \end{cases} \quad (4.3)$$

are the Blatt-Weisskopf form factors [33]. No dependence of the resonance parameters on the Blatt-Weisskopf radius R is found and it is therefore fixed to 2.5 GeV^{-1} . The quantity L is the angular momentum between the two decay fragments: $L = 1$ for P -wave, $L = 2$ for D -wave and $L = 3$ for F -wave resonances. The $D_{sJ}(3040)^+$ resonance is described by a nonrelativistic BW function multiplied by $P(m)$. The $D_{s2}^*(2573)^+$ parameters are fixed to the values obtained in the fit to the DK mass spectra [10]. The background is described by an empirical model [34],

$$B(m) = \begin{cases} P(m)e^{a_1 m + a_2 m^2} & \text{for } m < m_0, \\ P(m)e^{b_0 + b_1 m + b_2 m^2} & \text{for } m > m_0, \end{cases} \quad (4.4)$$

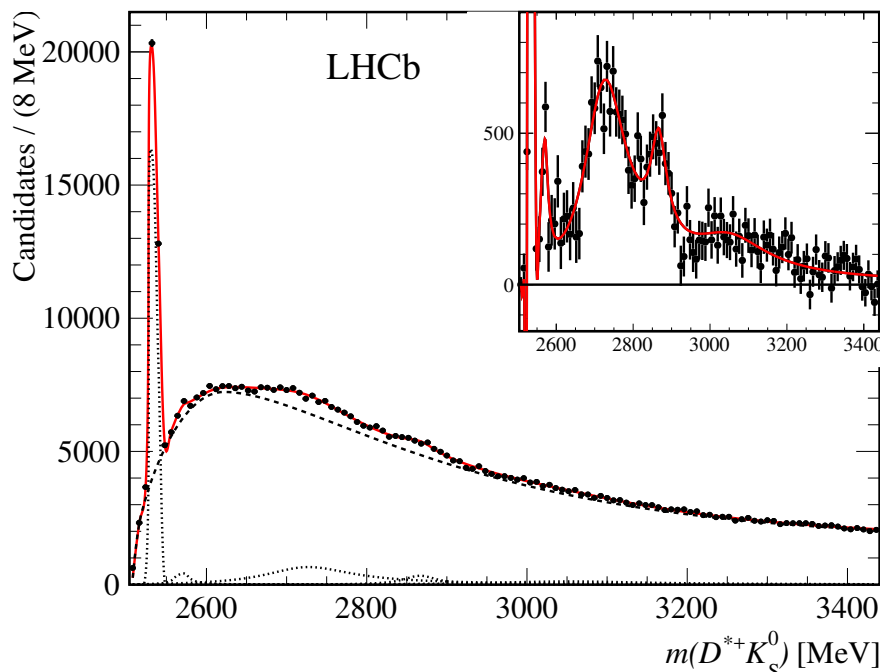


Figure 3. Distribution of the $D^{*+}K_S^0$ invariant mass for $D^0 \rightarrow K^-\pi^+$ decay. The full (red) line describes the fitting function. The dashed line displays the fitted background and the dotted lines the $D_{s1}(2536)^+$, $D_{s2}^*(2573)^+$, $D_{s1}^*(2700)^+$, $D_{sJ}^*(2860)^+$ and $D_{sJ}(3040)^+$ contributions. The inset displays the $D^{*+}K_S^0$ mass spectrum after subtracting the fitted background.

where $P(m)$ is described in eq. (3.5) and m_0 , $a_{i=1,2}$ and $b_{i=0,1,2}$ are free parameters. In eq. (4.4) we impose continuity to $B(m)$ and to its first derivative at the mass m_0 and therefore the number of free parameters is reduced by two. Resonances are included sequentially in order to test the χ^2 improvement when a new contribution is added. A better fit is obtained if a broad resonance in the 3000 MeV mass region is included. We find strong correlation between the parameters of this structure and the background and therefore we add the $D_{sJ}(3040)^+$ resonance in the fit with parameters fixed to the values obtained by BaBar [7].⁵

We also study the $D^{*+}K_S^0$ in the D^{*+} sideband region, defined as $2014.0 < m(D^0\pi^+) < 2018.1$ MeV. A smooth mass spectrum is obtained, well fitted by the above background model with no evidence for additional structures.

Table 1(a) gives the resulting $D_{s1}^*(2700)^+$ and $D_{sJ}^*(2860)^+$ fitted parameters. Statistical significances are computed as $S = \sqrt{\Delta\chi^2}$, where $\Delta\chi^2$ is the difference in χ^2 between fits with the resonance included and excluded from the fitting model. Large significances for $D_{s1}^*(2700)^+$ and $D_{sJ}^*(2860)^+$ are obtained, especially for the $D^0 \rightarrow K^-\pi^+$ decay mode. The significance of the $D_{sJ}(3040)^+$ enhancement is 2.4σ .

A search is performed for the $D_{s1}^*(2860)^+$ resonance previously observed in the $B_s^0 \rightarrow \bar{D}^0 K^-\pi^+$ Dalitz plot analysis [11, 12]. We first introduce in the fit an incoherent BW

⁵ $m(D_{sJ}(3040)^+) = 3044 \pm 8$ (stat) $_{-5}^{+30}$ (syst) MeV, $\Gamma(D_{sJ}(3040)^+) = 239 \pm 35$ (stat) $_{-42}^{+46}$ (syst) MeV.

Data		$D_{s1}^*(2700)^+$	$D_{sJ}^*(2860)^+$	χ^2/ndf
(a) $D^{*+}K_S^0$ $D^0 \rightarrow K^-\pi^+$	Mass	$2732.3 \pm 4.3 \pm 5.8$	$2867.1 \pm 4.3 \pm 1.9$	94/103
	Width	$136 \pm 19 \pm 24$	$50 \pm 11 \pm 13$	
	Yield	$(1.57 \pm 0.28) \times 10^4$	$(3.1 \pm 0.8) \times 10^3$	
	Significance	8.3	6.3	
(b) $D^{*+}K_S^0$ $D^0 \rightarrow K^-\pi^+$ NP sample	Mass	2729.3 ± 3.3	2861.2 ± 4.3	90/104
	Width	136 (fixed)	57 ± 14	
	Yield	$(1.50 \pm 0.11) \times 10^4$	$(2.50 \pm 0.60) \times 10^3$	
	Significance	7.6	7.1	
(c) $D^{*+}K_S^0$ $D^0 \rightarrow K^-\pi^+$ UP sample	Mass	2732.3 (fixed)	2876.7 ± 6.4	100/105
	Width	136 (fixed)	50 ± 19	
	Yield	$(0 \pm 0.8) \times 10^3$	$(1.0 \pm 0.4) \times 10^3$	
	Significance	0.0	3.6	
(d) $D^{*+}K_S^0$ $D^0 \rightarrow K^-\pi^+\pi^+\pi^-$	Mass	2725.5 ± 6.0	2844.0 ± 6.5	89/97
	Width	136 (fixed)	50 ± 15	
	Yield	$(2.6 \pm 0.4) \times 10^3$	490 ± 180	
	Significance	4.7	3.8	
(e) $D^{*0}K^+$	Mass	2728.3 ± 6.5	2860.9 ± 6.0	79/99
	Width	136 (fixed)	50 (fixed)	
	Yield	$(1.89 \pm 0.30) \times 10^3$	290 ± 90	
	Significance	6.6	3.1	

Table 1. Results from the fits to the $D^{*+}K_S^0$ and $D^{*0}K^+$ mass spectra. Resonances parameters are expressed in MeV. When two uncertainties are presented, the first is statistical and the second systematic. The symbol ndf indicates the number of degrees of freedom.

function with parameters free to vary within their statistical uncertainties around the reported values in ref. [11], but the fit returns a negligible contribution for this state. Since two $J^P = 1^-$ overlapping resonances may be present in the mass spectrum, interference is allowed between the $D_{s1}^*(2860)^+$ and the $D_{s1}^*(2700)^+$ resonance by including the amplitude

$$A_{1-} = |\text{BW}_{D_{s1}^*(2700)^+} + ce^{i\phi}\text{BW}_{D_{s1}^*(2860)^+}|^2 \quad (4.5)$$

where c and ϕ are free parameters. In this fit we also add the $D_{s3}^*(2860)^+$ resonance with parameters fixed to those from refs. [11, 12] and the $D_{s1}^*(2700)^+$ with parameters fixed to those from the DK analysis [10]. The resulting fit quality is similar to that obtained without the presence of the $D_{s1}^*(2860)^+$ resonance ($\chi^2/\text{ndf} = 92/103$). However it is found that the $D_{s1}^*(2860)^+$ is accommodated by the fit with strong destructive interference. We conclude that the data are not sensitive to the $D_{s1}^*(2860)^+$ resonance.

Systematic uncertainties on the resonance parameters are computed as quadratic sums of the differences between the nominal fit and fits in which the following changes are made.

- The alternative background function eq. (3.4) is used.

Source	$m(D_{s1}^*(2700)^+)$	$\Gamma(D_{s1}^*(2700)^+)$	$m(D_{sJ}^*(2860)^+)$	$\Gamma(D_{sJ}^*(2860)^+)$
Background function	5.0	19.4	1.7	12.7
Fit bias	0.2	1.6	0.2	1.5
$D_{sJ}(3040)^+$ parameters	1.3	5.7	0.5	3.2
Mass scale	0.3		0.5	
Fit model	2.6	12.0		
Total	5.8	23.6	1.9	13.2

Table 2. Contributions (in MeV) to the systematic uncertainties on the $D_{s1}^*(2700)^+$ and $D_{sJ}^*(2860)^+$ resonances parameters.

- The fit bias is evaluated by generating and fitting pseudoexperiments obtained using the parameters from the best fit. The deviations of the mean values of the distributions from the generated ones are taken as systematic uncertainties.
- The parameters of the $D_{sJ}(3040)^+$ state, fixed to the values of ref. [7] in all the fits, have been varied according to their total uncertainties.
- From the study of high-statistics control samples, a systematic uncertainty of $0.0015 Q$ on the mass scale is added, where Q is the Q -value involved in the resonance decay.
- The fitting model that includes the $D_{s1}^*(2860)^+$ resonance is tested with $D_{s3}^*(2860)^+$ parameters fixed and the $D_{s1}^*(2700)^+$ parameters left free.

The different contributions to the systematic uncertainties are summed in quadrature and are summarized in table 2. It can be noted that, combining statistical and systematic uncertainties, the resulting $D_{s1}^*(2700)^+$ mass is about 3σ higher than previous measurements while the $D_{sJ}^*(2860)^+$ parameters are consistent with those of the $D_{s3}^*(2860)^+$ resonance [32].

The angular distributions are expected to be proportional to $\sin^2 \theta_H$ for NP resonances and proportional to $1 + h \cos^2 \theta_H$ for UP resonances, where h is a free parameter. The D^*K decay is forbidden for a $J^P = 0^+$ resonance. Therefore the selection of candidates in different ranges of $\cos \theta_H$ can enhance or suppress different spin-parity contributions. We separate the $D^{*+}K_S^0$ data into two different categories, the NP sample, obtained with the selection $|\cos \theta_H| < 0.5$ and the UP sample, with the selection $|\cos \theta_H| > 0.5$.

The $D^{*+}K_S^0$ mass spectra for the NP sample is shown in figure 4(a), while the corresponding mass spectrum for the UP sample is shown in figure 4(b). Most resonant structures are in the NP sample. An enhancement in the 2860 MeV mass region in figure 4(b) indicates the possible presence of additional UP contributions. The fitted parameters are given in tables 1(b) and 1(c).

Figure 5(a) shows the $D^{*+}K_S^0$ mass spectrum for $D^0 \rightarrow K^-\pi^+\pi^+\pi^-$, which contains 3.92×10^4 combinations. Similar resonant structures to those seen for the $D^{*+}K_S^0$ final state with $D^0 \rightarrow K^-\pi^+$ are observed, albeit at lower significance. Table 1(d) provides the fitted resonance parameters. Due to the limited data samples, some parameters have been fixed

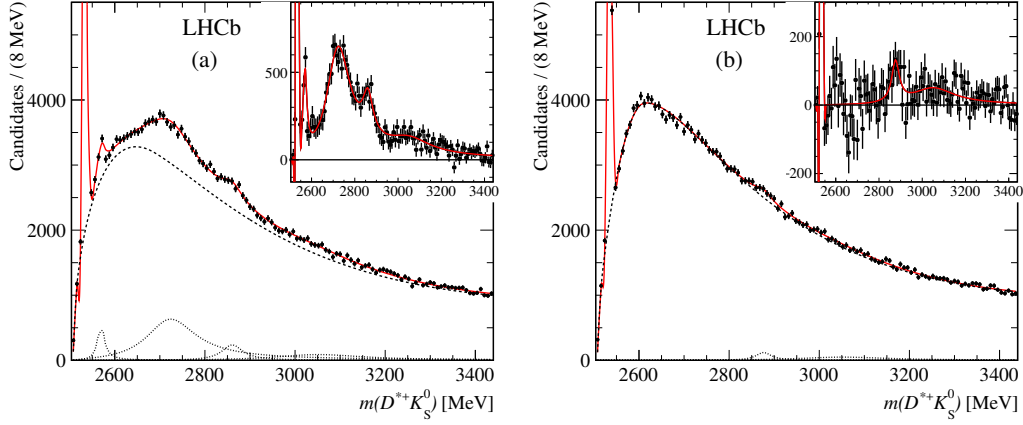


Figure 4. Mass spectrum of $D^{*+}K_S^0$ candidates for $D^0 \rightarrow K^-\pi^+$ in (a) the NP sample, and (b) the UP sample. The full (red) lines describe the fitting function. The dashed lines show the fitted background and the dotted lines the $D_{s2}^{*+}(2573)^+$, $D_{s1}^{*+}(2700)^+$, $D_{sJ}^{*+}(2860)^+$ and $D_{sJ}^{*+}(3040)^+$ contributions. The insets display the $D^{*+}K_S^0$ mass spectrum after subtracting the fitted background.

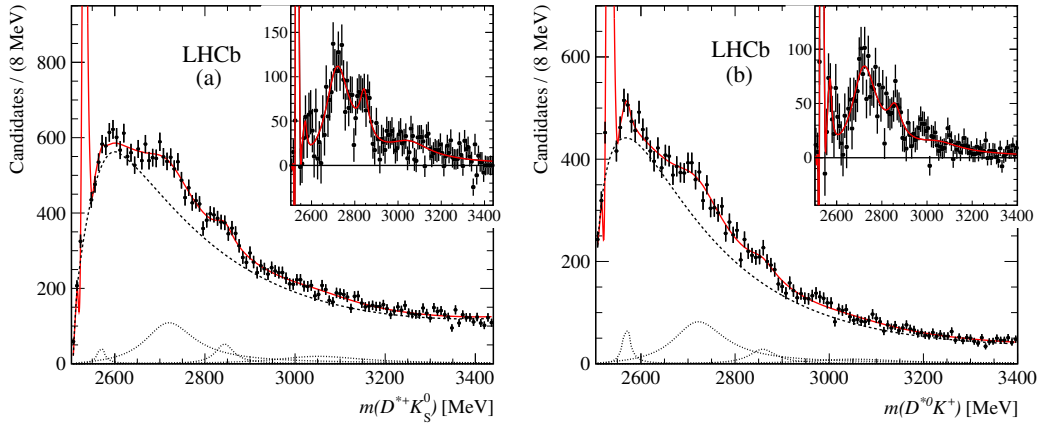


Figure 5. Mass spectrum of (a) $D^{*+}K_S^0$ candidates for $D^0 \rightarrow K^-\pi^+\pi^+\pi^-$, and (b) $D^{*0}K^+$ candidates for the NP sample. The full (red) lines describe the fitting function. The dashed lines show the fitted background and the dotted lines the $D_{s2}^{*+}(2573)^+$, $D_{s1}^{*+}(2700)^+$, $D_{sJ}^{*+}(2860)^+$ and $D_{sJ}^{*+}(3040)^+$ contributions. The insets display the $D^{*+}K_S^0$ and $D^{*0}K^+$ mass spectra after subtracting the fitted background.

to the values obtained from the fit to the $D^{*+}K_S^0$ sample with $D^0 \rightarrow K^-\pi^+$. The mass values are found to be consistent with the results from the other measurements.

The $D^{*0}K^+$ mass spectrum is affected by a high level of combinatorial background, mostly due to the D^{*0} reconstruction (see figure 2). As observed previously, the D^*K mass spectra are dominated by NP resonances and therefore in figure 5(b) we show the $D^{*0}K^+$ mass spectrum for the NP sample. The mass spectrum contains 2.53×10^4 combinations. We observe similar resonant structures as seen in the study of the $D^{*+}K_S^0$ mass spectra. The fitted resonance parameters are given in table 1(e); mass values are consistent with

the results from the fits to the other mass spectra. We do not have the sensitivity to the parameters of the $D_{s1}^*(2700)^+$ and $D_{s3}^*(2860)^+$ resonances in the fits to the $D^{*+}K_S^0$, $D^0 \rightarrow K^-\pi^+\pi^+\pi^-$, and $D^{*0}K^+$ mass spectra due to the low statistical significance of the signals.

5 Measurement of the branching fraction of the decay $D_{s2}^*(2573)^+ \rightarrow D^{*+}K_S^0$

We measure the branching fraction of the decay $D_{s2}^*(2573)^+ \rightarrow D^{*+}K_S^0$, $D^0 \rightarrow K^-\pi^+$ relative to that of the decay $D_{s2}^*(2573)^+ \rightarrow D^+K_S^0$. For this purpose the $D^+K_S^0$ mass spectrum from ref. [10], collected at 7 TeV with an integrated luminosity of 1 fb^{-1} , is re-fitted. In this study both long and downstream K_S^0 candidate types are used. The final states $D^{*+}K_S^0$, with $D^0 \rightarrow K^-\pi^+\pi^+\pi^-$ and $D^{*0}K^+$ are used as cross checks and to aid in determining the significance of the signal.

Figure 6 shows the $D^+K_S^0$ mass spectrum from ref. [10] along with the results of the fit described below. A narrow structure is seen near threshold, due to the cross-feed from the decay

$$D_{s1}(2536)^+ \rightarrow K_S^0 D^{*+} (\rightarrow D^+ \pi^0 / \gamma), \quad (5.1)$$

where the π^0/γ are not reconstructed. In the higher mass region, a strong $D_{s2}^*(2573)^+$ signal and a weak signal due to the $D_{s1}^*(2700)^+$ resonance are observed. Due to the difficulty of controlling the systematic uncertainties related to the determination of the relative efficiencies of the $D^{*+}K_S^0$ and $D^+K_S^0$ final states, we normalize the two mass spectra using the $D_{s1}(2536)^+$ signal which is observed as a peak in the $D^{*+}K_S^0$ and as cross-feed in the $D^+K_S^0$ final states.

The $D_{s2}^*(2573)^+$ resonance is a well known NP $J^P = 2^+$ state. To enhance the signal to background ratio, we plot in figure 7 the D^*K mass spectra for the NP sample of the three final states. All three distributions show a strong $D_{s1}(2536)^+$ signal and an enhancement at the $D_{s2}^*(2573)^+$ mass.

The $D^+K_S^0$ mass spectrum and the three D^*K mass spectra are fitted using the background function

$$B(m) = P(m)e^{\beta m + \gamma m^2}, \quad (5.2)$$

where $P(m)$ is given in eq. (3.5) and β and γ are free parameters. The $D_{s1}(2536)^+$ cross-feed into $D^+K_S^0$ is modelled using the sum of two Gaussian functions with the same mean, and the $D_{s2}^*(2573)^+$ resonance is modelled as a relativistic BW function convolved with a Gaussian function describing the experimental resolution ($\sigma = 3.5 \text{ MeV}$). Since the intrinsic width of the $D_{s1}(2536)^+$ state in the D^*K spectra is much smaller than the experimental resolution, the $D_{s1}(2536)^+$ is modelled using the sum of two Gaussian functions with the same mean. We obtain $m(D_{s1}(2536)^+) = 2535.00 \pm 0.01 \text{ MeV}$, in good agreement with the PDG average. The $D_{s2}^*(2573)^+$ resonance is modelled as a relativistic BW function convolved with the experimental resolution ($\sigma = 2.5 \text{ MeV}$ for $D_{s2}^*(2573)^+ \rightarrow D^{*+}K_S^0$, $D^0 \rightarrow K^-\pi^+$) taking the mass value as a free parameter and with the full width constrained to the value obtained from the fit to the $D^+K_S^0$ mass spectrum ($\Gamma = 17.5 \pm 0.4 \text{ MeV}$).

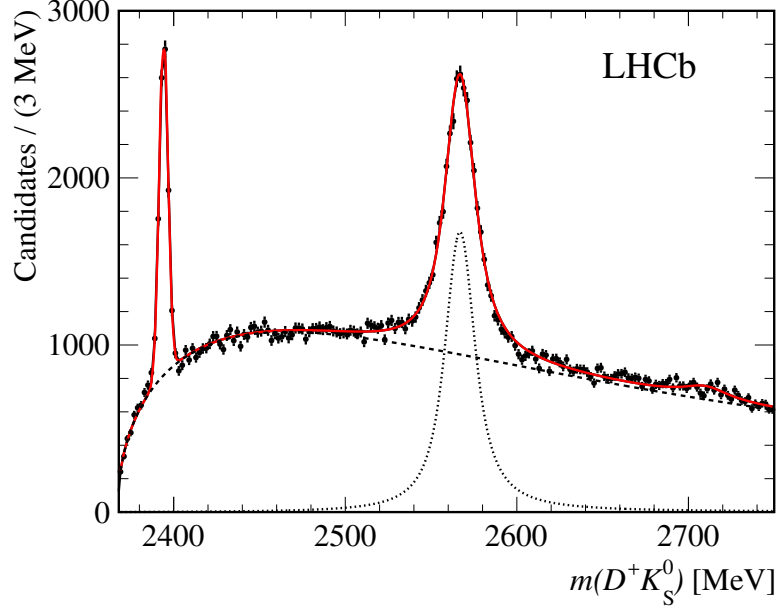


Figure 6. Distribution of the invariant mass of $D^+K_S^0$ candidates from ref. [10]. The full (red) line is the result from the fit described in the text. The dashed line indicates the fitted background and the dotted line shows the fitted $D_{s2}^*(2573)^+$ contribution.

Final state	Mass (MeV)	Γ (MeV)	Yield	Significance
$D_{s2}^*(2573)^+ \rightarrow D^+K_S^0$	2566.9 ± 0.1	17.5 ± 0.4	$(2.55 \pm 0.38) \times 10^4$	
$D_{s2}^*(2573)^+ \rightarrow D^{*+}K_S^0$ $D^0 \rightarrow K^-\pi^+$, NP	2568.0 ± 1.0	17.5 (fixed)	$(2.04 \pm 0.26) \times 10^3$	6.9σ
$D_{s2}^*(2573)^+ \rightarrow D^{*+}K_S^0$ $D^0 \rightarrow K^-\pi^+\pi^+\pi^-$, NP	2572.0 ± 1.3	17.5 (fixed)	$(5.0 \pm 1.0) \times 10^2$	4.6σ
$D_{s2}^*(2573)^+ \rightarrow D^{*0}K^+$	2567.3 ± 4.7	17.5 (fixed)	$(1.1 \pm 0.7) \times 10^2$	1.2σ
$D_{s1}(2536)^+ \rightarrow D^{*+}K_S^0$ $D^0 \rightarrow K^-\pi^+$, Total	2535.00 ± 0.01		$(3.59 \pm 0.15) \times 10^4$	

Table 3. Results from the fits to the $D^+K_S^0$ and $D^{*+}K_S^0$ mass spectra for the evaluation of the $D_{s2}^*(2573)^+ \rightarrow D^{*+}K_S^0$ relative branching fraction.

Table 3 summarizes the fit results. We note the large statistical significance of the $D_{s2}^*(2573)^+$ in the $D^{*+}K_S^0$ final states, especially for the sample with $D^0 \rightarrow K^-\pi^+$. Consistency is found, within the uncertainties, in the $D_{s2}^*(2573)^+$ mass measurements for the different final states. We therefore identify the observed structure as the first observation of the $D_{s2}^*(2573)^+ \rightarrow D^{*+}K_S^0$ decay.

The relative branching fraction

$$\mathcal{R} = \frac{\mathcal{B}(D_{s2}^*(2573)^+ \rightarrow D^{*+}K_S^0)}{\mathcal{B}(D_{s2}^*(2573)^+ \rightarrow D^+K_S^0)} \quad (5.3)$$

is determined using the results of fits to the $D_{s2}^*(2573)^+ \rightarrow D^{*+}K_S^0$, $D^0 \rightarrow K\pi$ data shown in figure 7(a) and the $D_{s2}^*(2573)^+ \rightarrow D^+K_S^0$ data shown in figure 6, summarized in table 3.

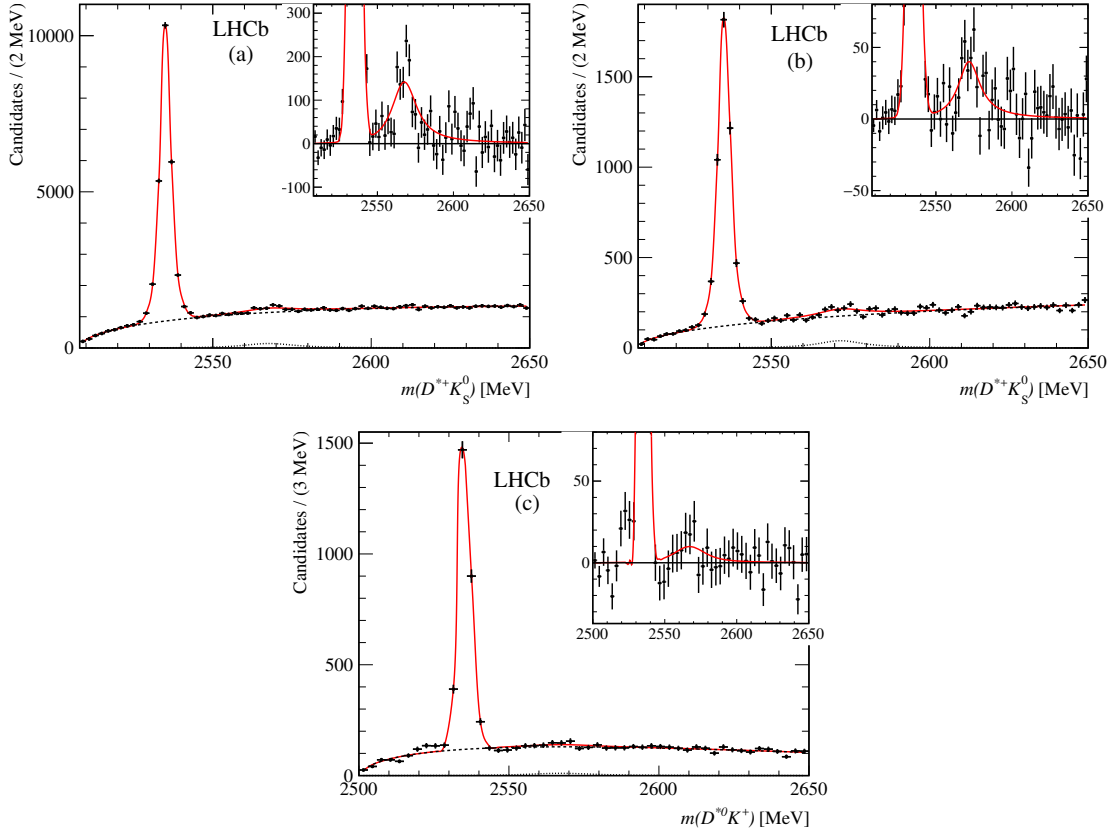


Figure 7. Mass spectra, in the $D_{s1}(2536)^+$ mass region, for the NP sample of (a) $D^{*+}K_S^0$ with $D^0 \rightarrow K^-\pi^+$, (b) $D^{*+}K_S^0$ with $D^0 \rightarrow K^-\pi^+\pi^+\pi^-$, and (c) $D^{*0}K^+$ final states. The full (red) lines describe the fitting function. The dashed lines show the fitted background and the dotted lines the $D_{s2}^*(2573)^+$ contributions. The insets display the D^*K mass spectra after subtracting the fitted background.

Using the $D^{*+}K_S^0$ final state, we verify that the $D_{s1}(2536)^+$ cross-feed into the $D^0K_S^0$ mass spectrum, when the pion from the D^{*+} decay is ignored, contains all the $D_{s1}(2536)^+$ signal. Similarly, using the $D^{*0}K^+$ data, we ignore the π^0 from the D^{*0} decay and plot the D^0K^+ mass spectrum. Also in this case, it is found that the $D_{s1}(2536)^+$ cross-feed contains all the decays in the $D_{s1}(2536)^+$ signal region. It is assumed that the $D_{s1}(2536)^+$ meson decay to D^*K is dominant. We test this hypothesis by studying the $D^0\pi^0K^+$ mass spectrum and find that no $D_{s1}(2536)^+$ signal is present outside the $D^{*0} \rightarrow D^0\pi^0$ signal region.

Indicating explicitly in brackets the D^{*+} decay modes, we define

$$R_1 = \frac{N(D_{s2}^*(2573)^+ \rightarrow (D^0\pi^+)K_S^0)}{N(D_{s1}(2536)^+ \rightarrow (D^0\pi^+)K_S^0)} \quad (5.4)$$

and

$$R_2 = \frac{N(D_{s1}(2536)^+ \rightarrow (D^+K_S^0)_f)}{N(D_{s2}^*(2573)^+ \rightarrow D^+K_S^0)}, \quad (5.5)$$

Quantities	Value
$N(D_{s2}^*(2573)^+ \rightarrow (D^0\pi^+)K_S^0)$	$(2.04 \pm 0.26 \text{ (stat)} \pm 0.14 \text{ (syst)}) \times 10^3$
$N(D_{s2}^*(2573)^+ \rightarrow D^+K_S^0)$	$(2.55 \pm 0.04 \text{ (stat)} \pm 0.08 \text{ (syst)}) \times 10^4$
$N(D_{s1}(2536)^+ \rightarrow (D^+K_S^0)_f)$	$(6.54 \pm 0.12 \text{ (stat)} \pm 0.05 \text{ (syst)}) \times 10^3$
$N(D_{s1}(2536)^+ \rightarrow (D^0\pi^+)K_S^0)$	$(3.59 \pm 0.15 \text{ (stat)} \pm 0.02 \text{ (syst)}) \times 10^4$
R_1	$0.057 \pm 0.006 \text{ (stat)} \pm 0.004 \text{ (syst)}$
R_2	$0.256 \pm 0.006 \text{ (stat)} \pm 0.008 \text{ (syst)}$
f_{NP}	1.45
B_D	$2.10 \pm 0.05 \text{ (stat)}$

Table 4. Measurements used to evaluate the $D_{s2}^*(2573)^+$ relative branching fraction $\mathcal{B}(D_{s2}^*(2573)^+ \rightarrow D^{*+}K_S^0)/\mathcal{B}(D_{s2}^*(2573)^+ \rightarrow D^+K_S^0)$.

where N indicates the yields and $D_{s1}(2536)^+ \rightarrow (D^+K_S^0)_f$ indicates the cross-feed from $D_{s1}(2536)^+ \rightarrow D^{*+}K_S^0$ where $D^{*+} \rightarrow D^+(\pi^0/\gamma)$ and the π^0/γ are undetected.

We measure the $D_{s2}^*(2573)^+$ relative branching ratio as

$$\mathcal{R} = R_1 \frac{\epsilon(D_{s1}(2536)^+ \rightarrow (D^0\pi^+)K_S^0)}{\epsilon(D_{s2}^*(2573)^+ \rightarrow (D^0\pi^+)K_S^0)} R_2 \frac{\epsilon(D_{s2}^*(2573)^+ \rightarrow D^+K_S^0)}{\epsilon(D_{s1}(2536)^+ \rightarrow (D^+K_S^0)_f)} B_D f_{\text{NP}}, \quad (5.6)$$

where ϵ indicates the efficiency for each final state. The ratio B_D , defined below, is taken from ref. [32],

$$B_D = \frac{\mathcal{B}(D^{*+} \rightarrow D^0\pi^+)}{\mathcal{B}(D^{*+} \rightarrow D^+(\pi^0/\gamma))} = 2.10 \pm 0.05, \quad (5.7)$$

where $D^+(\pi^0/\gamma)$ indicates both $D^+\pi^0$ and $D^+\gamma$ decays and f_{NP} is defined below.

In the evaluation of the $D_{s2}^*(2573)^+$ relative branching fraction, we make use of the $D^{*+}K_S^0$ NP sample. This selection is used to improve the signal to background ratio for the $D_{s2}^*(2573)^+$ resonance in the $D^{*+}K_S^0$ final state. We also fit the $D^{*+}K_S^0$ mass spectrum using the full dataset and we report the $D_{s1}(2536)^+$ yield indicated as Total in table 3. In eq. (5.6) the total $D_{s1}(2536)^+$ yield is used because of the unnatural parity of this state, and this requires a correction to the $D_{s2}^*(2573)^+$ yield for the effects of the NP sample selection. The angular distribution for a NP resonance is expected to be proportional to $\sin^2\theta_H$ and therefore the requirement $|\cos\theta_H| < 0.5$ selects 69% of the candidates. This correction in eq. (5.6) is included through the factor $f_{\text{NP}} = 1.45$.

In eq. (5.6) it can be noted that the efficiencies $\epsilon(D_{s2}^*(2573)^+ \rightarrow (D^0\pi^+)K_S^0)$ and $\epsilon(D_{s1}(2536)^+ \rightarrow (D^0\pi^+)K_S^0)$ involve the same final state. They are determined from simulation and are found to be the same within uncertainties. Similarly, the efficiencies $\epsilon(D_{s1}(2536)^+ \rightarrow (D^+K_S^0)_f)$ and $\epsilon(D_{s2}^*(2573)^+ \rightarrow (D^+K_S^0))$ are also found to be the same within uncertainties. Therefore, the efficiency ratios are set to unity.

Table 4 summarizes the measurements used to estimate the $D_{s2}^*(2573)^+$ relative branching fraction. We obtain

$$\mathcal{R} = \frac{\mathcal{B}(D_{s2}^*(2573)^+ \rightarrow D^{*+}K_S^0)}{\mathcal{B}(D_{s2}^*(2573)^+ \rightarrow D^+K_S^0)} = 0.044 \pm 0.005 \text{ (stat)} \pm 0.011 \text{ (syst)}. \quad (5.8)$$

Source	Value (%)
Datasets	22.2
Error on B_D	2.1
Efficiency	10.0
Resonance parameters and backgrounds	7.5
$D_{s2}^*(2573)^+$ width	0.3
Total	25.6

Table 5. Relative systematic uncertainties in the evaluation of the ratio of branching fractions \mathcal{R} .

The systematic uncertainty on the $D_{s2}^*(2573)^+$ relative branching fraction is computed as the quadratic sum of the differences between the reference values and those obtained when the following changes are made.

- The $D^+K_s^0$ data are collected at 7 TeV, while the $D^*K_s^0$ data include 7 TeV and 8 TeV data samples. We compute systematic uncertainties on the R_1 and R_2 ratios using the $D^*K_s^0$ at 7 TeV only and include the deviation in the systematic uncertainty.
- The uncertainty on the B_D parameter is propagated as a systematic uncertainty.
- Using simulation, we compute efficiency distributions as functions of $m(D^{*+}K_s^0)$ and $m(D^+K_s^0)$ and observe that they have weak variations in the regions used to evaluate the relative branching fraction. We assign a 10% systematic uncertainty to cover the assumptions that the efficiencies as functions of $m(D^{*+}K_s^0)$ and $m(D^+K_s^0)$ in eq. (5.6) are the same.
- We vary the shape of the background function using eq. (3.4) in the fits to the $D^{*+}K_s^0$ and $D^+K_s^0$ mass spectra and obtain new estimates for the resonance yields. We also remove the convolution with the resolution function or replace the relativistic BW functions with simple BW functions and include an additional Gaussian function to describe the $D_{s1}(2536)^+$ signal.
- We vary the $D_{s2}^*(2573)^+$ width by its statistical uncertainty (0.4 MeV) simultaneously in the fits to the $D^+K_s^0$ and $D^*K_s^0$ mass spectra.

The contributions to the systematic uncertainty are summarized in table 5 with the dominant component arising from the use of different datasets collected at different centre-of-mass energies.

We also perform a new estimate of the $D_{s2}^*(2573)^+$ significance in the $D^{*+}K_s^0$ final state by combining in quadrature the statistical and systematic uncertainties on the yield (see table 4) and obtain $S = N_{\text{signal}}/\sigma_{\text{tot}} = 6.9$, where σ_{tot} is the total error. This estimate is in good agreement with that reported in table 3.

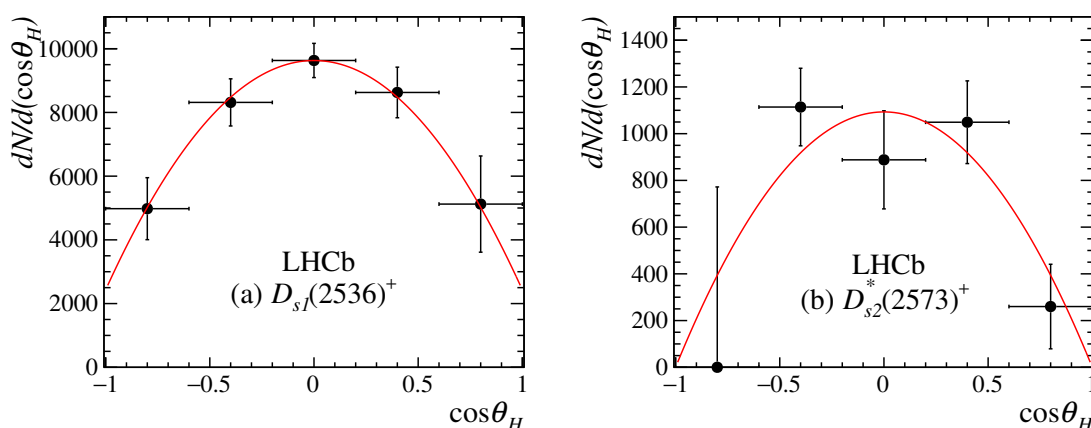


Figure 8. Distributions of the measured signal yields for (a) $D_{s1}(2536)^+$ and (b) $D_{s2}^*(2573)^+$ as a function of the helicity angle $\cos\theta_H$. The distributions are fitted with UP (a) and NP (b) functions.

Resonance	J^P	Function	χ^2/ndf
$D_{s1}(2536)^+$	1^+	$1 + h \cos^2 \theta_H$	0.1/3
$D_{s2}^*(2573)^+$	2^+	$\sin^2 \theta_H$	2.2/4
$D_{s1}^*(2700)^+$	1^-	$\sin^2 \theta_H$	11.4/7
$D_{s3}^*(2860)^+$	3^-	$\sin^2 \theta_H$	13.4/7
$D_{sJ}(3040)^+$	UP	$1 + h \cos^2 \theta_H$	8.0/6

Table 6. Values of χ^2/ndf from the fits to the helicity angles distributions.

6 Spin-parity analysis of the $D^{*+}K_S^0$ system

We obtain information on the spin-parity of the states observed in the $D^{*+}K_S^0$ mass spectrum. The data for $D^0 \rightarrow K^-\pi^+$ are first divided into five equally spaced bins in $\cos\theta_H$. The five mass spectra in the $D^{*+}K_S^0$ threshold region ($m(D^{*+}K_S^0) < 2650$ MeV) are fitted using the model described in section 5 with fixed $D_{s1}(2536)^+$ and $D_{s2}^*(2573)^+$ resonance parameters, to obtain the signal yields as functions of $\cos\theta_H$ for each resonance.

As stated previously, we determine from simulations that the efficiency as a function of $\cos\theta_H$ is consistent with being uniform; therefore we plot uncorrected angular distributions. The resulting distributions for $D_{s1}(2536)^+$ and $D_{s2}^*(2573)^+$ are shown in figure 8(a) and figure 8(b), and are fitted using the functions described in table 6. A good description of the data is obtained in terms of the expected angular distributions for $J^P = 1^+$ and $J^P = 2^+$ resonances. We note that the shape of the $D_{s1}(2536)^+$ angular distribution is in agreement with that measured in ref. [35].

The $D^{*+}K_S^0$ data, with $D^0 \rightarrow K^-\pi^+$, are then divided into eight equally spaced bins in $\cos\theta_H$. The mass spectra are fitted (for $m(D^{*+}K_S^0) < 3400$ MeV) with the model described in section 4 with fixed resonance parameters, to obtain the yields as functions of $\cos\theta_H$ for each resonance. The resulting distributions are shown in figure 9 and details of the fit results are given in table 6.

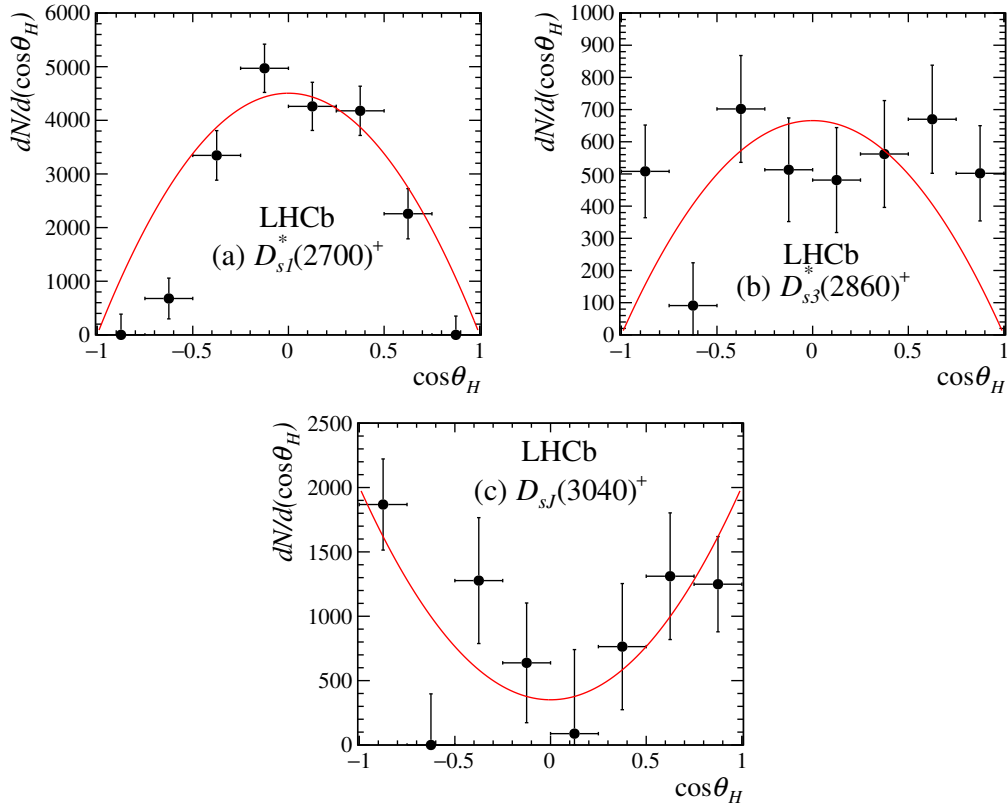


Figure 9. Distributions of the measured signal yields for (a) $D_{s1}^*(2700)^+$, (b) $D_{s3}^*(2860)^+$ and (c) $D_{sJ}(3040)^+$ as a function of the helicity angle $\cos\theta_H$. The distributions are fitted with NP (a,b) and UP (c) functions.

We observe that the $D_{s1}^*(2700)^+$ state is reasonably well described by the expected NP function ($\chi^2/\text{ndf} = 11.4/7$ with p-value 12.2%). The fit to the $D_{s3}^*(2860)^+$ angular distribution has a slightly lower p-value (6.3%). Reference [18] suggests the possibility of the presence of UP state contributions in this mass range, which cannot be excluded in this fit: there is evidence for the presence of a small signal in the 2860 MeV mass region for the UP sample shown in figure 4(b). The consistency with the NP assignment confirms the presence of the decay $D_{s3}^*(2860)^+ \rightarrow D^{*+}K_S^0$. We also show in figure 9(c) the $\cos\theta_H$ distribution for the enhancement at the $D_{sJ}(3040)^+$ position and find it consistent with a UP assignment.

7 Summary

A study of the resonant structures in the $D^{*+}K_S^0$ and $D^{*0}K^+$ systems is performed using pp collision data, collected at centre-of-mass energies of 7 and 8 TeV with the LHCb detector. For the $D^{*+}K_S^0$ final state, the decay chains $D^{*+} \rightarrow D^0\pi^+$ with $D^0 \rightarrow K^-\pi^+$ and $D^0 \rightarrow K^-\pi^+\pi^+\pi^-$ are used, with an integrated luminosity of 3.0 fb^{-1} . For $D^{*0}K^+$, the decay chain $D^{*0} \rightarrow D^0\pi^0$, $D^0 \rightarrow K^-\pi^+$ is used, with an integrated luminosity of 2.0 fb^{-1} .

A prominent $D_{s1}(2536)^+$ resonance is observed in both $D^{*+}K_s^0$ and $D^{*0}K^+$ final states. Resonances $D_{s1}^*(2700)^+$ and $D_{s3}^*(2860)^+$ are also observed and their parameters are measured to be

$$\begin{aligned} m(D_{s1}^*(2700)^+) &= 2732.3 \pm 4.3 \text{ (stat)} \pm 5.8 \text{ (syst)} \text{ MeV}, \\ \Gamma(D_{s1}^*(2700)^+) &= 136 \pm 19 \text{ (stat)} \pm 24 \text{ (syst)} \text{ MeV}, \end{aligned}$$

and

$$\begin{aligned} m(D_{sJ}^*(2860)^+) &= 2867.1 \pm 4.3 \text{ (stat)} \pm 1.9 \text{ (syst)} \text{ MeV}, \\ \Gamma(D_{sJ}^*(2860)^+) &= 50 \pm 11 \text{ (stat)} \pm 13 \text{ (syst)} \text{ MeV}. \end{aligned}$$

Study of the angular distributions supports natural parity assignments for both resonances, although the presence of an additional unnatural parity contribution in the 2860 MeV mass range cannot be excluded. The data are not sensitive to the presence of an additional $D_{s1}^*(2860)^+$ resonance.

The $D_{s2}^*(2573)^+$ decay to $D^{*+}K_s^0$ is also observed for the first time, at a significance of 6.9σ , with a branching fraction relative to the $D^+K_s^0$ decay mode of

$$\frac{\mathcal{B}(D_{s2}^*(2573)^+ \rightarrow D^{*+}K_s^0)}{\mathcal{B}(D_{s2}^*(2573)^+ \rightarrow D^+K_s^0)} = 0.044 \pm 0.005 \text{ (stat)} \pm 0.011 \text{ (syst)}. \quad (7.1)$$

This measurement is in agreement with expectations from recent calculations of the charm and charm-strange mesons spectra [21] which predict a value of 0.058 for this ratio. A spin-parity analysis of the decay $D_{s2}^*(2573)^+ \rightarrow D^{*+}K_s^0$ supports the natural parity assignment. The data also show weak evidence for further structure in the region around 3040 MeV consistent with contributions from unnatural parity states.

Acknowledgments

We express our gratitude to our colleagues in the CERN accelerator departments for the excellent performance of the LHC. We thank the technical and administrative staff at the LHCb institutes. We acknowledge support from CERN and from the national agencies: CAPES, CNPq, FAPERJ and FINEP (Brazil); NSFC (China); CNRS/IN2P3 (France); BMBF, DFG and MPG (Germany); INFN (Italy); FOM and NWO (The Netherlands); MNiSW and NCN (Poland); MEN/IFA (Romania); MinES and FANO (Russia); MinECo (Spain); SNSF and SER (Switzerland); NASU (Ukraine); STFC (United Kingdom); NSF (U.S.A.). We acknowledge the computing resources that are provided by CERN, IN2P3 (France), KIT and DESY (Germany), INFN (Italy), SURF (The Netherlands), PIC (Spain), GridPP (United Kingdom), RRCKI and Yandex LLC (Russia), CSCS (Switzerland), IFIN-HH (Romania), CBPF (Brazil), PL-GRID (Poland) and OSC (U.S.A.). We are indebted to the communities behind the multiple open source software packages on which we depend. Individual groups or members have received support from AvH Foundation (Germany), EPLANET, Marie Skłodowska-Curie Actions and ERC (European Union), Conseil Général de Haute-Savoie, Labex ENIGMASS and OCEVU, Région Auvergne (France), RFBR and Yandex LLC (Russia), GVA, XuntaGal and GENCAT (Spain), The Royal Society, Royal Commission for the Exhibition of 1851 and the Leverhulme Trust (United Kingdom).

Open Access. This article is distributed under the terms of the Creative Commons Attribution License ([CC-BY 4.0](https://creativecommons.org/licenses/by/4.0/)), which permits any use, distribution and reproduction in any medium, provided the original author(s) and source are credited.

References

- [1] BABAR collaboration, B. Aubert et al., *Observation of a narrow meson decaying to $D_s^+\pi^0$ at a mass of $2.32\text{ GeV}/c^2$* , *Phys. Rev. Lett.* **90** (2003) 242001 [[hep-ex/0304021](#)] [[INSPIRE](#)].
- [2] CLEO collaboration, D. Besson et al., *Observation of a narrow resonance of mass $2.46\text{ GeV}/c^2$ decaying to $D_s^{*+}\pi^0$ and confirmation of the $D_{sJ}^*(2317)$ state*, *Phys. Rev. D* **68** (2003) 032002 [Erratum *ibid.* **D 75** (2007) 119908] [[hep-ex/0305100](#)] [[INSPIRE](#)].
- [3] BELLE collaboration, K. Abe et al., *Measurements of the D_{sJ} resonance properties*, *Phys. Rev. Lett.* **92** (2004) 012002 [[hep-ex/0307052](#)] [[INSPIRE](#)].
- [4] BABAR collaboration, B. Aubert et al., *Observation of a narrow meson decaying to $D_s^+\pi^0\gamma$ at a mass of $2.458\text{ GeV}/c^2$* , *Phys. Rev. D* **69** (2004) 031101 [[hep-ex/0310050](#)] [[INSPIRE](#)].
- [5] N. Isgur and M.B. Wise, *Spectroscopy with heavy quark symmetry*, *Phys. Rev. Lett.* **66** (1991) 1130 [[INSPIRE](#)].
- [6] BABAR collaboration, B. Aubert et al., *Observation of a New D_s Meson Decaying to DK at a Mass of $2.86\text{ GeV}/c^2$* , *Phys. Rev. Lett.* **97** (2006) 222001 [[hep-ex/0607082](#)] [[INSPIRE](#)].
- [7] BABAR collaboration, B. Aubert et al., *Study of D_{sJ} decays to D^*K in inclusive e^+e^- interactions*, *Phys. Rev. D* **80** (2009) 092003 [[arXiv:0908.0806](#)] [[INSPIRE](#)].
- [8] BELLE collaboration, J. Brodzicka et al., *Observation of a new D_{sJ} meson $B^+ \rightarrow \bar{D}^0 D^0 K^+$ decays*, *Phys. Rev. Lett.* **100** (2008) 092001 [[arXiv:0707.3491](#)] [[INSPIRE](#)].
- [9] BABAR collaboration, J.P. Lees et al., *Dalitz plot analyses of $B^0 \rightarrow D^- D^0 K^+$ and $B^+ \rightarrow \bar{D}^0 D^0 K^+$ decays*, *Phys. Rev. D* **91** (2015) 052002 [[arXiv:1412.6751](#)] [[INSPIRE](#)].
- [10] LHCb collaboration, *Study of D_{sJ} decays to $D^+ K_S^0$ and $D^0 K^+$ final states in pp collisions*, *JHEP* **10** (2012) 151 [[arXiv:1207.6016](#)] [[INSPIRE](#)].
- [11] LHCb collaboration, *Observation of overlapping spin-1 and spin-3 $\bar{D}^0 K^-$ resonances at mass $2.86\text{ GeV}/c^2$* , *Phys. Rev. Lett.* **113** (2014) 162001 [[arXiv:1407.7574](#)] [[INSPIRE](#)].
- [12] LHCb collaboration, *Dalitz plot analysis of $B_s^0 \rightarrow \bar{D}^0 K^- \pi^+$ decays*, *Phys. Rev. D* **90** (2014) 072003 [[arXiv:1407.7712](#)] [[INSPIRE](#)].
- [13] P. Colangelo, F. De Fazio and S. Nicotri, *$D_{sJ}(2860)$ resonance and the $s_l^P = 5/2^- c\bar{s} (c\bar{q})$ doublet*, *Phys. Lett. B* **642** (2006) 48 [[hep-ph/0607245](#)] [[INSPIRE](#)].
- [14] F.E. Close, C.E. Thomas, O. Lakhina and E.S. Swanson, *Canonical interpretation of the $D_{sJ}(2860)$ and $D_{sJ}(2690)$* , *Phys. Lett. B* **647** (2007) 159 [[hep-ph/0608139](#)] [[INSPIRE](#)].
- [15] E. van Beveren and G. Rupp, *$D_{sJ}(2860)$ as the first radial excitation of $D_{s0}^*(2317)$* , *Phys. Rev. Lett.* **97** (2006) 202001 [[hep-ph/0606110](#)] [[INSPIRE](#)].
- [16] P. Colangelo, F. De Fazio, S. Nicotri and M. Rizzi, *Identifying $D_{sJ}(2700)$ through its decay modes*, *Phys. Rev. D* **77** (2008) 014012 [[arXiv:0710.3068](#)] [[INSPIRE](#)].
- [17] E. van Beveren and G. Rupp, *Comment on ‘Study of D_{sJ} decays to D^*K in inclusive e^+e^- interactions’*, *Phys. Rev. D* **81** (2010) 118101 [[arXiv:0908.1142](#)] [[INSPIRE](#)].

- [18] P. Colangelo, F. De Fazio, F. Giannuzzi and S. Nicotri, *New meson spectroscopy with open charm and beauty*, *Phys. Rev. D* **86** (2012) 054024 [[arXiv:1207.6940](#)] [[INSPIRE](#)].
- [19] R. Molina, T. Branz and E. Oset, *A new interpretation for the $D_{s2}^*(2573)$ and the prediction of novel exotic charmed mesons*, *Phys. Rev. D* **82** (2010) 014010 [[arXiv:1005.0335](#)] [[INSPIRE](#)].
- [20] S. Godfrey and I.T. Jardine, *Nature of the $D_{s1}^*(2710)$ and $D_{sJ}^*(2860)$ mesons*, *Phys. Rev. D* **89** (2014) 074023 [[arXiv:1312.6181](#)] [[INSPIRE](#)].
- [21] S. Godfrey and K. Moats, *Properties of Excited Charm and Charm-Strange Mesons*, [arXiv:1510.08305](#) [[INSPIRE](#)].
- [22] LHCb collaboration, *The LHCb Detector at the LHC*, *2008 JINST* **3** S08005 [[INSPIRE](#)].
- [23] LHCb collaboration, *LHCb Detector Performance*, *Int. J. Mod. Phys. A* **30** (2015) 1530022 [[arXiv:1412.6352](#)] [[INSPIRE](#)].
- [24] T. Sjöstrand, S. Mrenna and P.Z. Skands, *PYTHIA 6.4 Physics and Manual*, *JHEP* **05** (2006) 026 [[hep-ph/0603175](#)] [[INSPIRE](#)].
- [25] I. Belyaev et al., *Handling of the generation of primary events in Gauss, the LHCb simulation framework*, *J. Phys. Conf. Ser.* **331** (2011) 032047 [[INSPIRE](#)].
- [26] D.J. Lange, *The EvtGen particle decay simulation package*, *Nucl. Instrum. Meth. A* **462** (2001) 152 [[INSPIRE](#)].
- [27] P. Golonka and Z. Was, *PHOTOS Monte Carlo: A precision tool for QED corrections in Z and W decays*, *Eur. Phys. J. C* **45** (2006) 97 [[hep-ph/0506026](#)] [[INSPIRE](#)].
- [28] GEANT4 collaboration, J. Allison et al., *Geant4 developments and applications*, *IEEE Trans. Nucl. Sci.* **53** (2006) 270 [[INSPIRE](#)].
- [29] M. Clemencic et al., *The LHCb simulation application, Gauss: Design, evolution and experience*, *J. Phys. Conf. Ser.* **331** (2011) 032023 [[INSPIRE](#)].
- [30] GENBOD, CERN Program Library, <https://cern-tex.web.cern.ch/cern-tex/cernlib.html>.
- [31] M. Adinolfi et al., *Performance of the LHCb RICH detector at the LHC*, *Eur. Phys. J. C* **73** (2013) 2431 [[arXiv:1211.6759](#)] [[INSPIRE](#)].
- [32] PARTICLE DATA GROUP collaboration, K.A. Olive et al., *Review of Particle Physics*, *Chin. Phys. C* **38** (2014) 090001 [[INSPIRE](#)].
- [33] J. Blatt and V. E. Weisskopf, *Theoretical nuclear physics*, J. Wiley, New York (1952).
- [34] BABAR collaboration, P. del Amo Sanchez et al., *Observation of new resonances decaying to $D\pi$ and $D^*\pi$ in inclusive e^+e^- collisions near $\sqrt{s} = 10.58$ GeV*, *Phys. Rev. D* **82** (2010) 111101 [[arXiv:1009.2076](#)] [[INSPIRE](#)].
- [35] BELLE collaboration, V. Balagura et al., *Observation of $D_{s1}(2536)^+ \rightarrow D^+\pi^-K^+$ and angular decomposition of $D_{s1}(2536)^+ \rightarrow D^{*+}K_S^0$* , *Phys. Rev. D* **77** (2008) 032001 [[arXiv:0709.4184](#)] [[INSPIRE](#)].

The LHCb collaboration

R. Aaij³⁹, C. Abellán Beteta⁴¹, B. Adeva³⁸, M. Adinolfi⁴⁷, A. Affolder⁵³, Z. Ajaltouni⁵, S. Akar⁶, J. Albrecht¹⁰, F. Alessio³⁹, M. Alexander⁵², S. Ali⁴², G. Alkhazov³¹, P. Alvarez Cartelle⁵⁴, A.A. Alves Jr⁵⁸, S. Amato², S. Amerio²³, Y. Amhis⁷, L. An^{3,40}, L. Anderlini¹⁸, G. Andreassi⁴⁰, M. Andreotti^{17,g}, J.E. Andrews⁵⁹, R.B. Appleby⁵⁵, O. Aquines Gutierrez¹¹, F. Archilli³⁹, P. d'Argent¹², A. Artamonov³⁶, M. Artuso⁶⁰, E. Aslanides⁶, G. Auriemma^{26,n}, M. Baalouch⁵, S. Bachmann¹², J.J. Back⁴⁹, A. Badalov³⁷, C. Baesso⁶¹, W. Baldini^{17,39}, R.J. Barlow⁵⁵, C. Barschel³⁹, S. Barsuk⁷, W. Barter³⁹, V. Batzskaya²⁹, V. Battista⁴⁰, A. Bay⁴⁰, L. Beaucourt⁴, J. Beddow⁵², F. Bedeschi²⁴, I. Bediaga¹, L.J. Bel⁴², V. Belle⁴⁰, N. Belloli^{21,k}, I. Belyaev³², E. Ben-Haim⁸, G. Bencivenni¹⁹, S. Benson³⁹, J. Benton⁴⁷, A. Berezhnoy³³, R. Bernet⁴¹, A. Bertolin²³, M.-O. Bettler³⁹, M. van Beuzekom⁴², S. Bifani⁴⁶, P. Billoir⁸, T. Bird⁵⁵, A. Birnkraut¹⁰, A. Bizzeti^{18,i}, T. Blake⁴⁹, F. Blanc⁴⁰, J. Blouw¹¹, S. Blusk⁶⁰, V. Bocci²⁶, A. Bondar³⁵, N. Bondar^{31,39}, W. Bonivento¹⁶, S. Borghi⁵⁵, M. Borisyak⁶⁶, M. Borsato³⁸, T.J.V. Bowcock⁵³, E. Bowen⁴¹, C. Bozzi^{17,39}, S. Braun¹², M. Britsch¹², T. Britton⁶⁰, J. Brodzicka⁵⁵, N.H. Brook⁴⁷, E. Buchanan⁴⁷, C. Burr⁵⁵, A. Bursche⁴¹, J. Buytaert³⁹, S. Cadeddu¹⁶, R. Calabrese^{17,g}, M. Calvi^{21,k}, M. Calvo Gomez^{37,p}, P. Campana¹⁹, D. Campora Perez³⁹, L. Capriotti⁵⁵, A. Carbone^{15,e}, G. Carboni^{25,l}, R. Cardinale^{20,j}, A. Cardini¹⁶, P. Carniti^{21,k}, L. Carson⁵¹, K. Carvalho Akiba², G. Casse⁵³, L. Cassina^{21,k}, L. Castillo Garcia⁴⁰, M. Cattaneo³⁹, Ch. Cauet¹⁰, G. Cavallero²⁰, R. Cenci^{24,t}, M. Charles⁸, Ph. Charpentier³⁹, M. Chefdeville⁴, S. Chen⁵⁵, S.-F. Cheung⁵⁶, N. Chiapolini⁴¹, M. Chrzasczcz^{41,27}, X. Cid Vidal³⁹, G. Ciezarek⁴², P.E.L. Clarke⁵¹, M. Clemencic³⁹, H.V. Cliff⁴⁸, J. Closier³⁹, V. Coco³⁹, J. Cogan⁶, E. Cogneras⁵, V. Cogoni^{16,f}, L. Cojocariu³⁰, G. Collazuol^{23,r}, P. Collins³⁹, A. Comerma-Montells¹², A. Contu³⁹, A. Cook⁴⁷, M. Coombes⁴⁷, S. Coquereau⁸, G. Corti³⁹, M. Corvo^{17,g}, B. Couturier³⁹, G.A. Cowan⁵¹, D.C. Craik⁵¹, A. Crocombe⁴⁹, M. Cruz Torres⁶¹, S. Cunliffe⁵⁴, R. Currie⁵⁴, C. D'Ambrosio³⁹, E. Dall'Occo⁴², J. Dalseno⁴⁷, P.N.Y. David⁴², A. Davis⁵⁸, O. De Aguiar Francisco², K. De Bruyn⁶, S. De Capua⁵⁵, M. De Cian¹², J.M. De Miranda¹, L. De Paula², P. De Simone¹⁹, C.-T. Dean⁵², D. Decamp⁴, M. Deckenhoff¹⁰, L. Del Buono⁸, N. Déleage⁴, M. Demmer¹⁰, D. Derkach⁶⁶, O. Deschamps⁵, F. Dettori³⁹, B. Dey²², A. Di Canto³⁹, F. Di Ruscio²⁵, H. Dijkstra³⁹, S. Donleavy⁵³, F. Dordei³⁹, M. Dorigo⁴⁰, A. Dosil Suárez³⁸, A. Dovbnya⁴⁴, K. Dreimanis⁵³, L. Dufour⁴², G. Dujany⁵⁵, K. Dungs³⁹, P. Durante³⁹, R. Dzhelezhyan³⁶, A. Dziurda²⁷, A. Dzyuba³¹, S. Easo^{50,39}, U. Egede⁵⁴, V. Egorychev³², S. Eidelman³⁵, S. Eisenhardt⁵¹, U. Eitschberger¹⁰, R. Ekelhof¹⁰, L. Eklund⁵², I. El Rifai⁵, Ch. Elsasser⁴¹, S. Ely⁶⁰, S. Esen¹², H.M. Evans⁴⁸, T. Evans⁵⁶, M. Fabianska²⁷, A. Falabella¹⁵, C. Färber³⁹, N. Farley⁴⁶, S. Farry⁵³, R. Fay⁵³, D. Ferguson⁵¹, V. Fernandez Albor³⁸, F. Ferrari¹⁵, F. Ferreira Rodrigues¹, M. Ferro-Luzzi³⁹, S. Filippov³⁴, M. Fiore^{17,39,g}, M. Fiorini^{17,g}, M. Firlej²⁸, C. Fitzpatrick⁴⁰, T. Fiutowski²⁸, F. Fleuret^{7,b}, K. Fohl³⁹, P. Fol⁵⁴, M. Fontana¹⁶, F. Fontanelli^{20,j}, D. C. Forshaw⁶⁰, R. Forty³⁹, M. Frank³⁹, C. Frei³⁹, M. Frosini¹⁸, J. Fu²², E. Furfaro^{25,l}, A. Gallas Torreira³⁸, D. Galli^{15,e}, S. Gallorini²³, S. Gambetta⁵¹, M. Gandelman², P. Gandini⁵⁶, Y. Gao³, J. García Pardiñas³⁸, J. Garra Tico⁴⁸, L. Garrido³⁷, D. Gascon³⁷, C. Gaspar³⁹, R. Gauld⁵⁶, L. Gavardi¹⁰, G. Gazzoni⁵, D. Gerick¹², E. Gersabeck¹², M. Gersabeck⁵⁵, T. Gershon⁴⁹, Ph. Ghez⁴, S. Giani⁴⁰, V. Gibson⁴⁸, O.G. Girard⁴⁰, L. Giubega³⁰, V.V. Gligorov³⁹, C. Göbel⁶¹, D. Golubkov³², A. Golutvin^{54,39}, A. Gomes^{1,a}, C. Gotti^{21,k}, M. Grabalosa Gándara⁵, R. Graciani Diaz³⁷, L.A. Granado Cardoso³⁹, E. Graugés³⁷, E. Graverini⁴¹, G. Graziani¹⁸, A. Grecu³⁰, E. Greening⁵⁶, P. Griffith⁴⁶, L. Grillo¹², O. Grünberg⁶⁴, B. Gui⁶⁰, E. Gushchin³⁴, Yu. Guz^{36,39}, T. Gys³⁹, T. Hadavizadeh⁵⁶, C. Hadjivasiliou⁶⁰, G. Haefeli⁴⁰, C. Haen³⁹, S.C. Haines⁴⁸, S. Hall⁵⁴, B. Hamilton⁵⁹, X. Han¹², S. Hansmann-Menzemer¹², N. Harnew⁵⁶, S.T. Harnew⁴⁷, J. Harrison⁵⁵, J. He³⁹, T. Head⁴⁰,

V. Heijne⁴², A. Heister⁹, K. Hennessy⁵³, P. Henrard⁵, L. Henry⁸, J.A. Hernando Morata³⁸, E. van Herwijnen³⁹, M. Heß⁶⁴, A. Hicheur², D. Hill⁵⁶, M. Hoballah⁵, C. Hombach⁵⁵, W. Hulsbergen⁴², T. Humair⁵⁴, M. Hushchyn⁶⁶, N. Hussain⁵⁶, D. Hutchcroft⁵³, D. Hynds⁵², M. Idzik²⁸, P. Ilten⁵⁷, R. Jacobsson³⁹, A. Jaeger¹², J. Jalocha⁵⁶, E. Jans⁴², A. Jawahery⁵⁹, M. John⁵⁶, D. Johnson³⁹, C.R. Jones⁴⁸, C. Joram³⁹, B. Jost³⁹, N. Jurik⁶⁰, S. Kandybei⁴⁴, W. Kanso⁶, M. Karacson³⁹, T.M. Karbach^{39,†}, S. Karodia⁵², M. Kecke¹², M. Kelsey⁶⁰, I.R. Kenyon⁴⁶, M. Kenzie³⁹, T. Ketel⁴³, E. Khairullin⁶⁶, B. Khanji^{21,39,k}, C. Khurewathanakul⁴⁰, T. Kirn⁹, S. Klaver⁵⁵, K. Klimaszewski²⁹, O. Kochebina⁷, M. Kolpin¹², I. Komarov⁴⁰, R.F. Koopman⁴³, P. Koppenburg^{42,39}, M. Kozeiha⁵, L. Kravchuk³⁴, K. Kreplin¹², M. Kreps⁴⁹, P. Krokovny³⁵, F. Kruse¹⁰, W. Krzemien²⁹, W. Kucewicz^{27,o}, M. Kucharczyk²⁷, V. Kudryavtsev³⁵, A. K. Kuonen⁴⁰, K. Kurek²⁹, T. Kvaratskheliya³², D. Lacarrere³⁹, G. Lafferty^{55,39}, A. Lai¹⁶, D. Lambert⁵¹, G. Lanfranchi¹⁹, C. Langenbruch⁴⁹, B. Langhans³⁹, T. Latham⁴⁹, C. Lazzeroni⁴⁶, R. Le Gac⁶, J. van Leerdam⁴², J.-P. Lees⁴, R. Lefèvre⁵, A. Leflat^{33,39}, J. Lefrançois⁷, E. Lemos Cid³⁸, O. Leroy⁶, T. Lesiak²⁷, B. Leverington¹², Y. Li⁷, T. Likhomanenko^{66,65}, M. Liles⁵³, R. Lindner³⁹, C. Linn³⁹, F. Lionetto⁴¹, B. Liu¹⁶, X. Liu³, D. Loh⁴⁹, I. Longstaff⁵², J.H. Lopes², D. Lucchesi^{23,r}, M. Lucio Martinez³⁸, H. Luo⁵¹, A. Lupato²³, E. Luppi^{17,g}, O. Lupton⁵⁶, A. Lusiani²⁴, F. Machefert⁷, F. Maciuc³⁰, O. Maev³¹, K. Maguire⁵⁵, S. Malde⁵⁶, A. Malinin⁶⁵, G. Manca⁷, G. Mancinelli⁶, P. Manning⁶⁰, A. Mapelli³⁹, J. Maratas⁵, J.F. Marchand⁴, U. Marconi¹⁵, C. Marin Benito³⁷, P. Marino^{24,39,t}, J. Marks¹², G. Martellotti²⁶, M. Martin⁶, M. Martinelli⁴⁰, D. Martinez Santos³⁸, F. Martinez Vidal⁶⁷, D. Martins Tostes², L.M. Massacrier⁷, A. Massafferri¹, R. Matev³⁹, A. Mathad⁴⁹, Z. Mathe³⁹, C. Matteuzzi²¹, A. Mauri⁴¹, B. Maurin⁴⁰, A. Mazurov⁴⁶, M. McCann⁵⁴, J. McCarthy⁴⁶, A. McNab⁵⁵, R. McNulty¹³, B. Meadows⁵⁸, F. Meier¹⁰, M. Meissner¹², D. Melnychuk²⁹, M. Merk⁴², E. Michielin²³, D.A. Milanes⁶³, M.-N. Minard⁴, D.S. Mitzel¹², J. Molina Rodriguez⁶¹, I.A. Monroy⁶³, S. Monteil⁵, M. Morandin²³, P. Morawski²⁸, A. Mordà⁶, M.J. Morello^{24,t}, J. Moron²⁸, A.B. Morris⁵¹, R. Mountain⁶⁰, F. Muheim⁵¹, D. Müller⁵⁵, J. Müller¹⁰, K. Müller⁴¹, V. Müller¹⁰, M. Mussini¹⁵, B. Muster⁴⁰, P. Naik⁴⁷, T. Nakada⁴⁰, R. Nandakumar⁵⁰, A. Nandi⁵⁶, I. Nasteva², M. Needham⁵¹, N. Neri²², S. Neubert¹², N. Neufeld³⁹, M. Neuner¹², A.D. Nguyen⁴⁰, T.D. Nguyen⁴⁰, C. Nguyen-Mau^{40,q}, V. Niess⁵, R. Niet¹⁰, N. Nikitin³³, T. Nikodem¹², A. Novoselov³⁶, D.P. O'Hanlon⁴⁹, A. Oblakowska-Mucha²⁸, V. Obraztsov³⁶, S. Ogilvy⁵², O. Okhrimenko⁴⁵, R. Oldeman^{16,48,f}, C.J.G. Onderwater⁶⁸, B. Osorio Rodrigues¹, J.M. Otalora Goicochea², A. Otto³⁹, P. Owen⁵⁴, A. Oyanguren⁶⁷, A. Palano^{14,d}, F. Palombo^{22,u}, M. Palutan¹⁹, J. Panman³⁹, A. Papanestis⁵⁰, M. Pappagallo⁵², L.L. Pappalardo^{17,g}, C. Pappenheimer⁵⁸, W. Parker⁵⁹, C. Parkes⁵⁵, G. Passaleva¹⁸, G.D. Patel⁵³, M. Patel⁵⁴, C. Patrignani^{20,j}, A. Pearce^{55,50}, A. Pellegrino⁴², G. Penso^{26,m}, M. Pepe Altarelli³⁹, S. Perazzini^{15,e}, P. Perret⁵, L. Pescatore⁴⁶, K. Petridis⁴⁷, A. Petrolini^{20,j}, M. Petruzzo²², E. Picatoste Olloqui³⁷, B. Pietrzyk⁴, M. Pikies²⁷, D. Pinci²⁶, A. Pistone²⁰, A. Piucci¹², S. Playfer⁵¹, M. Plo Casasus³⁸, T. Poikela³⁹, F. Polci⁸, A. Poluektov^{49,35}, I. Polyakov³², E. Polcarpo², A. Popov³⁶, D. Popov^{11,39}, B. Popovici³⁰, C. Potterat², E. Price⁴⁷, J.D. Price⁵³, J. Prisciandaro³⁸, A. Pritchard⁵³, C. Prouve⁴⁷, V. Pugatch⁴⁵, A. Puig Navarro⁴⁰, G. Punzi^{24,s}, W. Qian⁴, R. Quagliani^{7,47}, B. Rachwal²⁷, J.H. Rademacker⁴⁷, M. Rama²⁴, M. Ramos Pernas³⁸, M.S. Rangel², I. Raniuk⁴⁴, N. Rauschmayr³⁹, G. Raven⁴³, F. Redi⁵⁴, S. Reichert⁵⁵, A.C. dos Reis¹, V. Renaudin⁷, S. Ricciardi⁵⁰, S. Richards⁴⁷, M. Rihl³⁹, K. Rinnert^{53,39}, V. Rives Molina³⁷, P. Robbe^{7,39}, A.B. Rodrigues¹, E. Rodrigues⁵⁵, J.A. Rodriguez Lopez⁶³, P. Rodriguez Perez⁵⁵, S. Roiser³⁹, V. Romanovsky³⁶, A. Romero Vidal³⁸, J. W. Ronayne¹³, M. Rotondo²³, T. Ruf³⁹, P. Ruiz Valls⁶⁷, J.J. Saborido Silva³⁸, N. Sagidova³¹, B. Saitta^{16,f}, V. Salustino Guimaraes², C. Sanchez Mayordomo⁶⁷, B. Sanmartin Sedes³⁸, R. Santacesaria²⁶, C. Santamarina Rios³⁸, M. Santimaria¹⁹, E. Santovetti^{25,l}, A. Sarti^{19,m}, C. Satriano^{26,n},

A. Satta²⁵, D.M. Saunders⁴⁷, D. Savrina^{32,33}, S. Schael⁹, M. Schiller³⁹, H. Schindler³⁹, M. Schlupp¹⁰, M. Schmelling¹¹, T. Schmelzer¹⁰, B. Schmidt³⁹, O. Schneider⁴⁰, A. Schopper³⁹, M. Schubiger⁴⁰, M.-H. Schune⁷, R. Schwemmer³⁹, B. Sciascia¹⁹, A. Sciubba^{26,m}, A. Semennikov³², A. Sergi⁴⁶, N. Serra⁴¹, J. Serrano⁶, L. Sestini²³, P. Seyfert²¹, M. Shapkin³⁶, I. Shapoval^{17,44,g}, Y. Shcheglov³¹, T. Shears⁵³, L. Shekhtman³⁵, V. Shevchenko⁶⁵, A. Shires¹⁰, B.G. Siddi¹⁷, R. Silva Coutinho⁴¹, L. Silva de Oliveira², G. Simi^{23,s}, M. Sirendi⁴⁸, N. Skidmore⁴⁷, T. Skwarnicki⁶⁰, E. Smith^{56,50}, E. Smith⁵⁴, I.T. Smith⁵¹, J. Smith⁴⁸, M. Smith⁵⁵, H. Snoek⁴², M.D. Sokoloff^{58,39}, F.J.P. Soler⁵², F. Soomro⁴⁰, D. Souza⁴⁷, B. Souza De Paula², B. Spaan¹⁰, P. Spradlin⁵², S. Sridharan³⁹, F. Stagni³⁹, M. Stahl¹², S. Stahl³⁹, S. Stefkova⁵⁴, O. Steinkamp⁴¹, O. Stenyakin³⁶, S. Stevenson⁵⁶, S. Stoica³⁰, S. Stone⁶⁰, B. Storaci⁴¹, S. Stracka^{24,t}, M. Straticiuc³⁰, U. Straumann⁴¹, L. Sun⁵⁸, W. Sutcliffe⁵⁴, K. Swientek²⁸, S. Swientek¹⁰, V. Syropoulos⁴³, M. Szczekowski²⁹, T. Szumlak²⁸, S. T'Jampens⁴, A. Tayduganov⁶, T. Tekampe¹⁰, G. Tellarini^{17,g}, F. Teubert³⁹, C. Thomas⁵⁶, E. Thomas³⁹, J. van Tilburg⁴², V. Tisserand⁴, M. Tobin⁴⁰, J. Todd⁵⁸, S. Tolk⁴³, L. Tomassetti^{17,g}, D. Tonelli³⁹, S. Topp-Joergensen⁵⁶, N. Torr⁵⁶, E. Tournefier⁴, S. Tourneur⁴⁰, K. Trabelsi⁴⁰, M. Traill⁵², M.T. Tran⁴⁰, M. Tresch⁴¹, A. Trisovic³⁹, A. Tsaregorodtsev⁶, P. Tsopelas⁴², N. Tuning^{42,39}, A. Ukleja²⁹, A. Ustyuzhanin^{66,65}, U. Uwer¹², C. Vacca^{16,39,f}, V. Vagnoni¹⁵, G. Valenti¹⁵, A. Vallier⁷, R. Vazquez Gomez¹⁹, P. Vazquez Regueiro³⁸, C. Vázquez Sierra³⁸, S. Vecchi¹⁷, M. van Veghel⁴³, J.J. Velthuis⁴⁷, M. Veltri^{18,h}, G. Veneziano⁴⁰, M. Vesterinen¹², B. Viaud⁷, D. Vieira², M. Vieites Diaz³⁸, X. Vilasis-Cardona^{37,p}, V. Volkov³³, A. Vollhardt⁴¹, D. Voong⁴⁷, A. Vorobyev³¹, V. Vorobyev³⁵, C. Voß⁶⁴, J.A. de Vries⁴², R. Waldi⁶⁴, C. Wallace⁴⁹, R. Wallace¹³, J. Walsh²⁴, J. Wang⁶⁰, D.R. Ward⁴⁸, N.K. Watson⁴⁶, D. Websdale⁵⁴, A. Weiden⁴¹, M. Whitehead³⁹, J. Wicht⁴⁹, G. Wilkinson^{56,39}, M. Wilkinson⁶⁰, M. Williams³⁹, M.P. Williams⁴⁶, M. Williams⁵⁷, T. Williams⁴⁶, F.F. Wilson⁵⁰, J. Wimberley⁵⁹, J. Wishahi¹⁰, W. Wislicki²⁹, M. Witek²⁷, G. Wormser⁷, S.A. Wotton⁴⁸, K. Wraight⁵², S. Wright⁴⁸, K. Wyllie³⁹, Y. Xie⁶², Z. Xu⁴⁰, Z. Yang³, J. Yu⁶², X. Yuan³⁵, O. Yushchenko³⁶, M. Zangoli¹⁵, M. Zavertyaev^{11,c}, L. Zhang³, Y. Zhang³, A. Zhelezov¹², A. Zhokhov³², L. Zhong³, V. Zhukov⁹ and S. Zucchelli¹⁵

¹ Centro Brasileiro de Pesquisas Físicas (CBPF), Rio de Janeiro, Brazil

² Universidade Federal do Rio de Janeiro (UFRJ), Rio de Janeiro, Brazil

³ Center for High Energy Physics, Tsinghua University, Beijing, China

⁴ LAPP, Université Savoie Mont-Blanc, CNRS/IN2P3, Annecy-Le-Vieux, France

⁵ Clermont Université, Université Blaise Pascal, CNRS/IN2P3, LPC, Clermont-Ferrand, France

⁶ CPPM, Aix-Marseille Université, CNRS/IN2P3, Marseille, France

⁷ LAL, Université Paris-Sud, CNRS/IN2P3, Orsay, France

⁸ LPNHE, Université Pierre et Marie Curie, Université Paris Diderot, CNRS/IN2P3, Paris, France

⁹ I. Physikalisches Institut, RWTH Aachen University, Aachen, Germany

¹⁰ Fakultät Physik, Technische Universität Dortmund, Dortmund, Germany

¹¹ Max-Planck-Institut für Kernphysik (MPIK), Heidelberg, Germany

¹² Physikalisches Institut, Ruprecht-Karls-Universität Heidelberg, Heidelberg, Germany

¹³ School of Physics, University College Dublin, Dublin, Ireland

¹⁴ Sezione INFN di Bari, Bari, Italy

¹⁵ Sezione INFN di Bologna, Bologna, Italy

¹⁶ Sezione INFN di Cagliari, Cagliari, Italy

¹⁷ Sezione INFN di Ferrara, Ferrara, Italy

¹⁸ Sezione INFN di Firenze, Firenze, Italy

¹⁹ Laboratori Nazionali dell'INFN di Frascati, Frascati, Italy

²⁰ Sezione INFN di Genova, Genova, Italy

²¹ Sezione INFN di Milano Bicocca, Milano, Italy

²² Sezione INFN di Milano, Milano, Italy

²³ Sezione INFN di Padova, Padova, Italy

- ²⁴ *Sezione INFN di Pisa, Pisa, Italy*
- ²⁵ *Sezione INFN di Roma Tor Vergata, Roma, Italy*
- ²⁶ *Sezione INFN di Roma La Sapienza, Roma, Italy*
- ²⁷ *Henryk Niewodniczanski Institute of Nuclear Physics Polish Academy of Sciences, Kraków, Poland*
- ²⁸ *AGH – University of Science and Technology, Faculty of Physics and Applied Computer Science, Kraków, Poland*
- ²⁹ *National Center for Nuclear Research (NCBJ), Warsaw, Poland*
- ³⁰ *Horia Hulubei National Institute of Physics and Nuclear Engineering, Bucharest-Magurele, Romania*
- ³¹ *Petersburg Nuclear Physics Institute (PNPI), Gatchina, Russia*
- ³² *Institute of Theoretical and Experimental Physics (ITEP), Moscow, Russia*
- ³³ *Institute of Nuclear Physics, Moscow State University (SINP MSU), Moscow, Russia*
- ³⁴ *Institute for Nuclear Research of the Russian Academy of Sciences (INR RAN), Moscow, Russia*
- ³⁵ *Budker Institute of Nuclear Physics (SB RAS) and Novosibirsk State University, Novosibirsk, Russia*
- ³⁶ *Institute for High Energy Physics (IHEP), Protvino, Russia*
- ³⁷ *Universitat de Barcelona, Barcelona, Spain*
- ³⁸ *Universidad de Santiago de Compostela, Santiago de Compostela, Spain*
- ³⁹ *European Organization for Nuclear Research (CERN), Geneva, Switzerland*
- ⁴⁰ *Ecole Polytechnique Fédérale de Lausanne (EPFL), Lausanne, Switzerland*
- ⁴¹ *Physik-Institut, Universität Zürich, Zürich, Switzerland*
- ⁴² *Nikhef National Institute for Subatomic Physics, Amsterdam, The Netherlands*
- ⁴³ *Nikhef National Institute for Subatomic Physics and VU University Amsterdam, Amsterdam, The Netherlands*
- ⁴⁴ *NSC Kharkiv Institute of Physics and Technology (NSC KIPT), Kharkiv, Ukraine*
- ⁴⁵ *Institute for Nuclear Research of the National Academy of Sciences (KINR), Kyiv, Ukraine*
- ⁴⁶ *University of Birmingham, Birmingham, United Kingdom*
- ⁴⁷ *H.H. Wills Physics Laboratory, University of Bristol, Bristol, United Kingdom*
- ⁴⁸ *Cavendish Laboratory, University of Cambridge, Cambridge, United Kingdom*
- ⁴⁹ *Department of Physics, University of Warwick, Coventry, United Kingdom*
- ⁵⁰ *STFC Rutherford Appleton Laboratory, Didcot, United Kingdom*
- ⁵¹ *School of Physics and Astronomy, University of Edinburgh, Edinburgh, United Kingdom*
- ⁵² *School of Physics and Astronomy, University of Glasgow, Glasgow, United Kingdom*
- ⁵³ *Oliver Lodge Laboratory, University of Liverpool, Liverpool, United Kingdom*
- ⁵⁴ *Imperial College London, London, United Kingdom*
- ⁵⁵ *School of Physics and Astronomy, University of Manchester, Manchester, United Kingdom*
- ⁵⁶ *Department of Physics, University of Oxford, Oxford, United Kingdom*
- ⁵⁷ *Massachusetts Institute of Technology, Cambridge, MA, United States*
- ⁵⁸ *University of Cincinnati, Cincinnati, OH, United States*
- ⁵⁹ *University of Maryland, College Park, MD, United States*
- ⁶⁰ *Syracuse University, Syracuse, NY, United States*
- ⁶¹ *Pontifícia Universidade Católica do Rio de Janeiro (PUC-Rio), Rio de Janeiro, Brazil, associated to ²*
- ⁶² *Institute of Particle Physics, Central China Normal University, Wuhan, Hubei, China, associated to ³*
- ⁶³ *Departamento de Física, Universidad Nacional de Colombia, Bogota, Colombia, associated to ⁸*
- ⁶⁴ *Institut für Physik, Universität Rostock, Rostock, Germany, associated to ¹²*
- ⁶⁵ *National Research Centre Kurchatov Institute, Moscow, Russia, associated to ³²*
- ⁶⁶ *Yandex School of Data Analysis, Moscow, Russia, associated to ³²*
- ⁶⁷ *Instituto de Física Corpuscular (IFIC), Universitat de Valencia-CSIC, Valencia, Spain, associated to ³⁷*
- ⁶⁸ *Van Swinderen Institute, University of Groningen, Groningen, The Netherlands, associated to ⁴²*

- ^a *Universidade Federal do Triângulo Mineiro (UFTM), Uberaba-MG, Brazil*
- ^b *Laboratoire Leprince-Ringuet, Palaiseau, France*
- ^c *P.N. Lebedev Physical Institute, Russian Academy of Science (LPI RAS), Moscow, Russia*
- ^d *Università di Bari, Bari, Italy*
- ^e *Università di Bologna, Bologna, Italy*
- ^f *Università di Cagliari, Cagliari, Italy*
- ^g *Università di Ferrara, Ferrara, Italy*
- ^h *Università di Urbino, Urbino, Italy*
- ⁱ *Università di Modena e Reggio Emilia, Modena, Italy*
- ^j *Università di Genova, Genova, Italy*
- ^k *Università di Milano Bicocca, Milano, Italy*
- ^l *Università di Roma Tor Vergata, Roma, Italy*
- ^m *Università di Roma La Sapienza, Roma, Italy*
- ⁿ *Università della Basilicata, Potenza, Italy*
- ^o *AGH – University of Science and Technology, Faculty of Computer Science, Electronics and Telecommunications, Kraków, Poland*
- ^p *LIFAELS, La Salle, Universitat Ramon Llull, Barcelona, Spain*
- ^q *Hanoi University of Science, Hanoi, Viet Nam*
- ^r *Università di Padova, Padova, Italy*
- ^s *Università di Pisa, Pisa, Italy*
- ^t *Scuola Normale Superiore, Pisa, Italy*
- ^u *Università degli Studi di Milano, Milano, Italy*
- [†] *Deceased*